LAWRENCE
LIVERMORE
NATIONAL
LABORATORY

LLNL-SR-677422

Neutronics Evaluation of Lithium-Based Ternary Alloys in IFE Blankets

A. Jolodosky, M. Fratoni

September 22, 2015

Disclaimer

This work performed under the auspices of the U.S. Department of Energy by Lawrence Livermore National Laboratory under Contract DE-AC52-07NA27344.

Neutronics Evaluation of Lithium-Based Ternary Alloys in IFE Blankets

Alejandra Jolodosky and Massimiliano Fratoni
University of California, Berkeley
FY 2015 Report

1. Introduction

Lithium is often the preferred choice as breeder and coolant in fusion blankets as it offers excellent heat transfer and corrosion properties, and most importantly, it has a very high tritium solubility and results in very low levels of tritium permeation throughout the facility infrastructure [1]. However, lithium metal vigorously reacts with air and water and exacerbates plant safety concerns [2]. For this reason, over the years numerous blanket concepts have been proposed with the scope of reducing concerns associated with lithium [3-4]. The European helium cooled pebble bed breeding blanket (HCPB) physically confines lithium within ceramic pebbles [3]. The pebbles reside within a low activation martensitic ferritic steel structure and are cooled by helium. The blanket is composed of the tritium breeding lithium ceramic pebbles and neutron multiplying beryllium pebbles. Other blanket designs utilize lead to lower chemical reactivity [5]; LiPb alone can serve as a breeder, coolant, neutron multiplier, and tritium carrier. Blankets employing LiPb coolants alongside silicon carbide structural components can achieve high plant efficiency, low afterheat, and low operation pressures [3]. This alloy can also be used alongside of helium such as in the dual-coolant lead-lithium concept (DCLL); helium is utilized to cool the first wall and structural components made up of low-activation ferritic steel, whereas lithium-lead (LiPb) acts as a self-cooled breeder in the inner channels of the blanket [3]. The helium-cooled steel and lead-lithium alloy are separated by flow channel inserts (usually made out of silicon carbide) which thermally insulate the self-cooled breeder region from the helium cooled steel walls. This creates a LiPb breeder with a much higher exit temperature than the steel which increases the power cycle efficiency and also lowers the magnetohydrodynamic (MHD) pressure drop [6]. Molten salt blankets with a mixture of lithium, beryllium, and fluorides (FLiBe) offer good tritium breeding, low electrical conductivity and therefore low MHD pressure drop, low chemical reactivity, and extremely low tritium inventory [3]; the addition of sodium (FLiNaBe) has been considered because it retains the properties of FliBe but also lowers the melting point [4]. Although many of these blanket concepts are promising, challenges still remain. The limited amount of beryllium available poses a problem for ceramic breeders such as the HCPB. FLiBe and FLiNaBe are highly viscous and have a low thermal conductivity. Lithium lead possesses a poor thermal conductivity which can cause problems in both DCLL and LiPb blankets. Additionally, the tritium permeation from these two blankets into plant components can be a problem and must be reduced [3]. Consequently, Lawrence Livermore National Laboratory (LLNL) is attempting to develop a lithium-based alloy—most likely a ternary alloy—which maintains the beneficial properties of lithium (e.g. high tritium breeding and solubility) while reducing overall flammability concerns for use in the blanket of an inertial fusion energy (IFE) power plant [7-8]. The LLNL concept employs inertial confinement fusion (ICF) through the use of lasers aimed at an indirect-driven target composed of deuterium-tritium fuel. The fusion driver/target design implements the same physics currently experimented at the National Ignition Facility (NIF). The plant uses lithium in both the primary coolant and blanket; therefore, lithium-related hazards are of primary concern. Although reducing chemical reactivity is the primary motivation for the development of new lithium alloys, the successful candidates will have to guarantee acceptable performance in all their functions. The scope of this study is to evaluate the neutronics performance of a large number of lithium-based alloys in the blanket of the IFE engine and assess their properties upon activation. This manuscript is organized as follows: Section 1~~2~~ presents the models and methodologies used for the analysis; Section 3 discusses the results; Section 4 summarizes findings and future work.

2. Models and Methodology

2.1. Chamber Model

The neutronics performance of each alloy was evaluated in the blanket of an IFE power plant. The blanket is built around the fusion chamber that consists of a central spherical cavity with a 13.004 m radius. Fusion occurs at the center of the void chamber where the laser beams impact the fuel target. The ICF target releases 132 MJ from

D(T,n)α reactions; 97.45 MJ is in neutrons kinetic energy and 34.55 MJ is in x-rays and ions [9]. The target also releases $4.69 \cdot 10^{19}$ neutrons from fusion and additional $0.13 \cdot 10^{19}$ neutrons (2.8% of the total) from (n,2n) reactions with the compressed DT fuel and the lead hohlraum. Alpha particles instantly deposit their energy in the surrounding DT fuel, in the ablator materials, and in the lead capsule resulting in the release of x-rays and ions [10]. Xenon fills the void chamber at a density of 6 μg/cm^3 and shields the chamber wall (first wall) from ions and x-rays [9]. The blanket surrounds the central chamber and consists of a series of coolant/breeder layers separated by structural components (Table 1). The structural material is HT9 (composed of iron (85.9%), chromium (12.1%), and the rest is carbon, silicon niobium, molybdenum, and tungsten with density of 8 g/cm^3); it features high resistance against radiation damage and low chemical reactivity. In the original design the coolant/breeder material is lithium; this study replaces lithium with a ternary lithium alloy. The blanket is completed by a 100 cm graphite reflector (1.7 g/cm^3). The plant is assumed to generate 2,200 MW of fusion power.

Table 1 Composition and dimensions of the blanket components.

Layer, #	Material	Thickness (cm)
1	HT9	0.5
2	Breeder/Coolant	1
3	HT9	0.5
4	Breeder/Coolant	100
5	HT9	0.5
6	Breeder/Coolant	50
7	HT9	0.5
8	Graphite	100

Neutron and photon transport calculations were performed using the three-dimensional Monte Carlo transport code MCNP6 [11]. A simplified model consisting of concentric spherical regions was assumed (Figure 1). The model also includes 42 penetrations through the blanket representing the beam ports, as well, the target injection port at the top of the chamber and the debris exit port at the bottom. Modeling the indirect-driver and target is extremely complex, and for the scope of this study the DT target was represented as a point source at the center of the chamber with a neutron energy distribution as obtained in accurate target models (Figure 2). The energy spectrum accounts for the scattering of the fusion neutrons with the DT target and lead hohlraum. All materials in the model utilized ENDF/B-VII.I cross sections at 900 K [12].

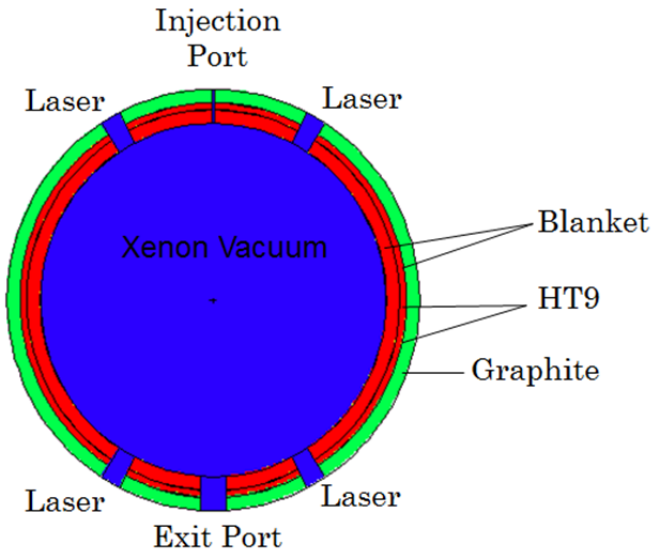

Figure 1: MCNP model of the IFE chamber viewed from the xz plane.

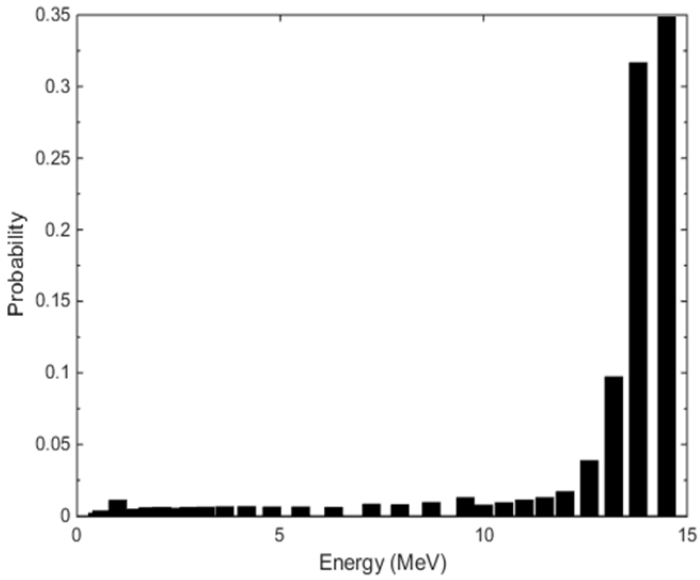

Figure 2: Fusion source neutron energy distribution [13].

The neutronics performance of the alloys was evaluated by two parameters: (1) tritium breeding ratio (TBR), and (2) energy multiplication factor (EMF). TBR is defined as the ratio of tritium produced in the blanket to the tritium consumed in the target [14]. Tritium production was calculated through tallies in the MCNP model. The TBR must be greater than unity for the system to be self-sufficient and account for losses in the design including the first wall, blanket structure, penetrations, and decay after extraction. Earlier studies on the IFE design assumed a minimum TBR constrain of 1.02. This is lower than what other fusion plants require due to the high fractional burn-up (~30%) in the IFE source and lower tritium permeation in the lithium alloy coolant [15]. EMF is defined as the ratio of power deposited in the blanket and other regions outside the IFE chamber by neutrons, gammas, and alpha particles to the power generated from fusion reactions [16]. It is given by:

$$EMF = \frac{E_d + E_\alpha}{E_f} \quad (1)$$

where E_d is the total energy deposited in the chamber (first wall, breeding regions, structures, and reflector) and surrounding regions (shield, beam dumps, etc.) as the result of neutron reactions; E_α is the energy of the x-rays and ions (from alpha interactions) absorbed in the chamber gas and subsequently the first wall—this is calculated to be 4.607 MeV; E_f is the total fusion energy released per D-T reaction (17.6 MeV). The neutron and neutron induced gamma energy deposited in regions outside the chamber is included with the expectation that this power will be recovered and will contribute to the overall power cycle. There is no hard physical constraint on the EMF, but the higher the EMF, the lower the cost of electricity from a fusion power plant due to more power available for a given target and laser of certain size. For this reason, a goal of at least 1.1 was set for the EMF.

2.2. Activation Analysis

The high neutron flux to which the blanket is exposed activates its components. As the coolant circulates outside of the blanket it requires operational and maintenance procedures appropriate to its radiological properties. Furthermore, accumulation in the coolant of relative long-lived isotopes will determine its nuclear waste category and the corresponding procedures for disposal. Neutron activation analysis was performed using ACAB [17], an activation and transmutation specifically developed for fusion systems. Multigroup activation cross section libraries are selected from one of the group-wise libraries available inEAF-2007 [18] group-wise libraries. These multi-group files are gathered from a point-wise cross section library in one out of seven group structures; this study used the VITAMISN-J, 175 group structure. This group structure was defined in the framework of the JEF-1 benchmarking for use in reactor shielding and fusion neutronics application (fusion blanket shielding). It is based on the group structures of VITAMIN-C (DLC-41) and VITAMIN-E (DLC-113). VITAMIN-J has 175 neutron energy groups and 42 gamma energy groups [19]. The point-wise library contains data on 65,565 cross sections on 816 targets in modified ENDF/B format ranging from 10^{-5} eV to 60 MeV. The EAF-2007 decay data library is primarily based on the JEFF-3.1 radioactive decay data library [18]. MCNP6 provided the multi-group flux required by ACAB for collapsing cross sections. Activation analysis was performed for a 2,200 MW plant with an irradiation history of 50 years and cooling time of up to 300 years. One important thing to note is that the total blanket volume includes the 3,478 m^3 inside the chamber, and the 940 m^3 outside. This means that the alloy is inside the chamber for 79% of the total residence time. To account for this, the flux is multiplied by 0.79. The results are then multiplied by the inverse to account for the entire blanket volume irradiated. Another consideration was to account for ^{6}Li depletion and decrease of TBR by feeding more lithium into the system. However, the amount of ^{6}Li atoms consumed during irradiation only ranged from 2%-8% for the different alloys analyzed, and the TBR only decreased by less than 1% by the end of the irradiation time. Consequently, feeding more lithium into the chamber during operation is not necessary. Tritium is assumed to be extracted from the coolant/breeder after irradiation to be reprocessed and reused in the source. Many of the activation safety parameters are examined after shutdown and thus do not include tritium in the results. The only exception is the accident dose since an accident is assumed to occur for the fraction of the coolant/breeder that resides inside the chamber and during operation.

2.3. Safety and Environmental Parameters

Data from the activation analysis allowed to determine the following environmental and safety parameters.

Decay heat

Decay heat is calculated to ensure that adequate cooling is available for stored coolant at all times. According to limits employed in previous studies, no-active cooling is required if the decay heat is below 10 W/m^3, dry cooling is sufficient if it is between 10 W/m^3 and 2 kW/m^3, and wet cooling is required above 2 kW/m^3 [20].

Contact dose rate

The contact dose rate determines the dose to workers handling a given material. The proposed limits for fusion systems are 10 μSv/h for hands on operation, and 10 mSv/h for remote handling [21]. More detailed work has also suggested the same 10 μSv/h hands on limit, but also includes a shielded hands on limit of 2 mSv/h [20]. For this study, the hands on limit was disregarded since the coolant after shutdown could be drained down into cooling tanks. Remote handling, instead, will be required at the least to transport the coolant to the waste site.

Waste disposal rating

The waste disposal rating (WDR) determines whether a material can be disposed via shallow land burial [22]. The WDR is calculated using isotope specific activity limits; for each isotope, a ratio of the calculated concentration to the limiting concentration is determined. The sum over all radionuclides gives the material WDR. If the WDR is greater than one, the material does not meet the class C requirements for shallow land burial.

Accident dose

DOE Fusion Safety Standards limit dose in accident scenario to 10 mSv [23]. This value refers to a 50 year committed effective dose calculated to the most exposed individual at the site boundary (1 km) with contributions from direct cloudshine, and inhalation during plume passage [24]. The contribution from groundshine is not included in the limit because it doesn't contribute directly to the accident and is more of public health measure. Nevertheless, this study will include groundshine for more conservative results. The accident dose (AD) is calculated by multiplying the following three factors:

$$AD = Radioactivity\,(Bq) \times DCF\left(\frac{Sv}{Bq}\right) \times RF \qquad (2)$$

The radioactivity is obtained from ACAB calculations. Dose conversion factors (DCFs) are required to convert the radioactivity levels from the released blanket radionuclides to equivalent dose to humans. DCFs for typical radionuclides released from IFE activation of structural materials were specifically calculated using the dispersion and accident consequences software MACCS2 [24]. For this study, the DCFs were chosen with standard conditions such as a 1 km boundary, conservative weather, ground release, and no building wake effects. The release fractions (RF) are usually derived from the combination of detailed modeling of the accident and measurements of the material mobilization under such accident conditions. This determines how much of the component escapes from the accident, and what percentage of that is released into the atmosphere and pose a hazard to the public. Modeling detailed accident scenarios for each alloy would take too long. Approximated release fractions, instead, were utilized. Such release fractions characterize an isotope's mobilization and volatility according to five categories [25]:

1. Elements with species gaseous at room temperature: high mobility – 100%
2. Elements with species gaseous at typical reactor operating temperatures (<500°C) – 30%
3. Elements with species gaseous at modest accident temperatures (<1000°C) – 10%
4. Elements with species gaseous at severe accident temperature (<1500°C) – 3%
5. Elements with species (pure element or oxide) at severe gaseous temperatures such as tokamak dust erosion or oxide spallation – 1%

3. Results and Discussion

3.1. Preliminary Evaluations

In order to understand the behavior of different elements in the blanket, preliminary evaluations were performed. Using a representative blanket neutron flux (obtained from MCNP calculations with a LiSnZn alloy), effective q-value, effective absorption cross section, and effective (n,xn) cross section were calculated. The effective q-value was calculated as:

$$Q_e = \frac{\sum_{i=1}^{N_e} a^i \sum_r Q_r^i \sigma_r^i}{\sum_{i=1}^{N_e} a^i \sum_r \sigma_r^i} \qquad (2)$$

$$Q_{(n,xn)}^i = Q_{(n,xn)} + xQ_e^{Li} \qquad (3)$$

where i is the specific isotope of an element, r is the type of neutron reaction, σ is the cross section, Q is the q-value, a is the abundance fraction, and Ne is the number of isotopes in the element. It is assumed that the x (2 or 3) neutrons generated in (n,xn) reactions will go on to be absorbed by lithium and this is accounted for in the q-value defined in Equation (3). From a neutronics perspective, it is desirable to have low absorption cross section to reduce neutron loss, large (n,xn) cross section to increase the number of neutrons in the blanket, and high effective q-value to enhance EMF. The last two features contradict each other as (n,xn) reactions are endothermic, but overall the availability of extra neutrons upon (n,xn) reaction may compensate the loss of energy due to subsequent exothermic reaction with ^{6}Li and/or other alloy constituents. An initial set of elements (sodium, magnesium, aluminum, silicon, calcium, titanium, copper, zinc, gallium, strontium, palladium, silver, indium, tin, antimony, barium, gold, lead, and bismuth) was selected by the LLNL based on thermodynamics properties [26]. Results reported in Table 2 show that: lead and bismuth are desirable elements for their low absorption and high (n,xn) cross sections, but have small q-values; of the elements with high q-value, tin, zinc, copper, and titanium are to be preferred for their relative low absorption.

Table 2: Effective cross sections and q-values for selected elements.

Element	q-value, MeV	Absorption cross section, b	(n,xn) cross section, b
Lithium	4.67	7.37E-02	1.53E-03
Lithium-6	4.78	9.77E-01	0.00E+00
Lithium-7	-7.16	4.63E-04	1.66E-03
Sodium	-1.79	1.53E-02	5.30E-04
Magnesium	-2.13	2.35E-02	4.77E-03
Aluminum	-0.96	1.57E-02	1.21E-04
Silicon	-2.67	3.21E-02	9.30E-04
Calcium	0.48	5.39E-02	5.31E-04
Titanium	3.47	2.78E-02	1.45E-02
Copper	5.12	7.24E-02	2.20E-02
Zinc	4.44	5.97E-02	1.24E-02
Gallium	5.45	1.33E-01	3.25E-02
Strontium	1.97	1.59E-02	3.11E-02
Palladium	6.86	3.72E-01	7.24E-02
Silver	6.37	6.50E-01	6.36E-02
Indium	6.2	6.68E-01	6.76E-02
Tin	4.18	7.51E-02	7.34E-02
Antimony	5.61	3.65E-01	6.82E-02
Barium	3.55	5.14E-02	7.99E-02
Gold	5.76	6.98E-01	1.07E-01
Lead	1.76	5.58E-03	1.17E-01
Bismuth	1.64	6.37E-03	1.14E-01

The elements above were also observed in combination with lithium. Binary alloys were analyzed using the MCNP blanket model and varying the lithium concentration from 0 to 100% at 5% intervals. This analysis assumed 1.02 and 1.1 as lower limits for TBR and EMF, respectively. Figure 3 shows example results for LiSn and LiPb binary alloys (a complete set is provided in Appendix A). It is observed that: (1) Ba, Sn, Sr, and Ti offer the widest range of acceptable lithium concentration; (2) Bi and Pb barely do not meet the EMF requirement, but provide very large TBR even at low concentration of lithium, due to enhanced (n,xn) reactions. Studies in the past demonstrated the potential of LiPb as a coolant and breeder. However, TBR was the metric usually considered with lithium enriched to boost it [27]; (3) Pd, In, Au, and Ag feature a narrow acceptable range, but a relatively large EMF; (4) Ga, Cu, Sb and Zn are in the mid-range of acceptable lithium compositions with EMFs slightly higher than 1.1 but no greater than 1.2; (5) Sb, Pd and Au have very narrow acceptable ranges and limited EMF; (6) Na, Mg, Al, Ca, and Si never meet both constraints, mainly due to their detrimental effect on EMF. These results are in line with the observations made from the analysis on individual elements.

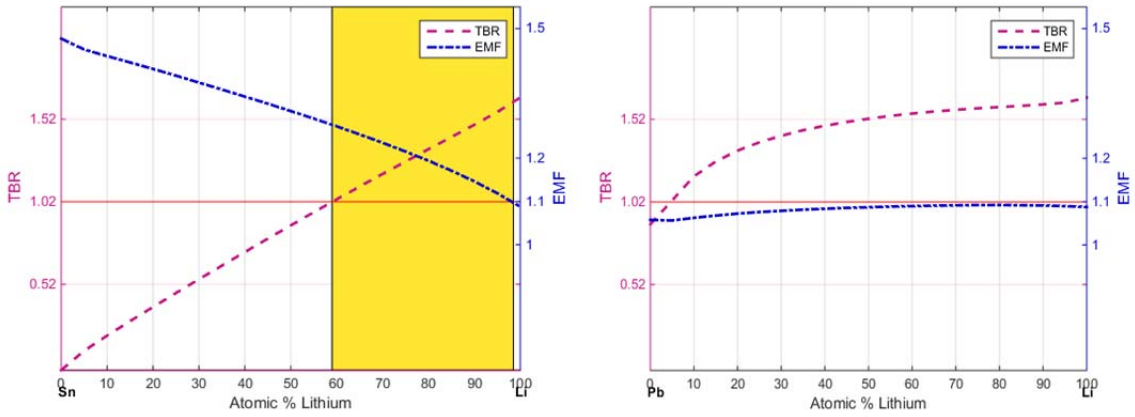

(a) (b)

Figure 3: TBR and EMF for lithium (a) LiSn and (b) LiPb alloys as a function of lithium concentration; the horizontal red line coincides with the minimum value for both TBR (1.02) and EMF (1.10), the shaded yellow area indicates the range of lithium concentration within which both constraints are met.

3.2. Tritium breeding and energy multiplication

TBR and EMF were evaluated for 55 lithium ternary alloys as a function of their composition. Each alloy was evaluated according to three different TBR and EMF criteria:

- Aggressive: lowest achievable TBR – 1.02 and highest EMF – 1.2. This category pushes limits to ideal conditions; a TBR that accounts for the least amount of losses and a high EMF to decrease the cost of electricity.
- Conservative: high TBR – 1.1 and low EMF – 1.1. More on the other side of the spectrum, the TBR is high to account for losses, and EMF puts the lowest demand to produce power.
- Semi-conservative (SC): TBR – 1.05 and EMF – 1.1. The TBR here is lowered from the conservative constrain above.

Results containing the range lithium concentrations for various ternary alloys that meet each of the three sets of criteria are illustrated in Figure 4.

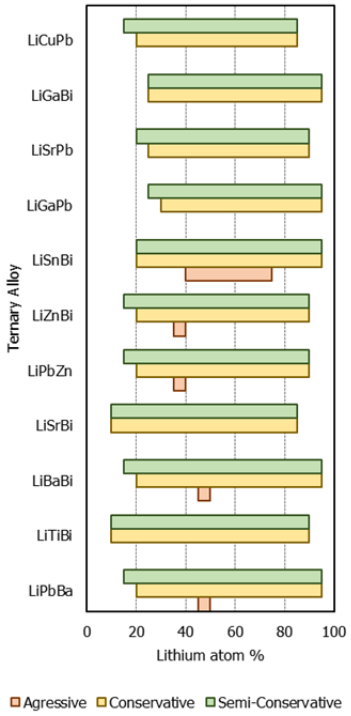
LiCuPb
LiGaBi
LiSrPb
LiGaPb
LiSnBi
LiZnBi
LiPbZn
LiSrBi
LiBaBi
LiTiBi
LiPbBa
Ternary Alloy
0
20
40
60
80
100
Lithium atom %
Agressive
Conservative
Semi-Conservative

(a)

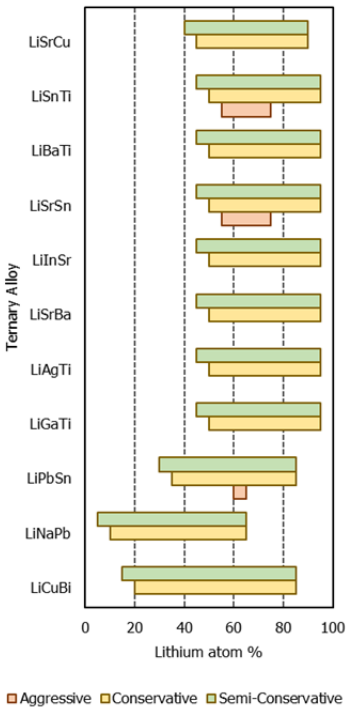
LiSrCu
LiSnTi
LiBaTi
LiSrSn
LiInSr
LiSrBa
LiAgTi
LiGaTi
LiPbSn
LiNaPb
LiCuBi
Ternary Alloy
0
20
40
60
80
100
Lithium atom %
Aggressive
Conservative
Semi-Conservative

(b)

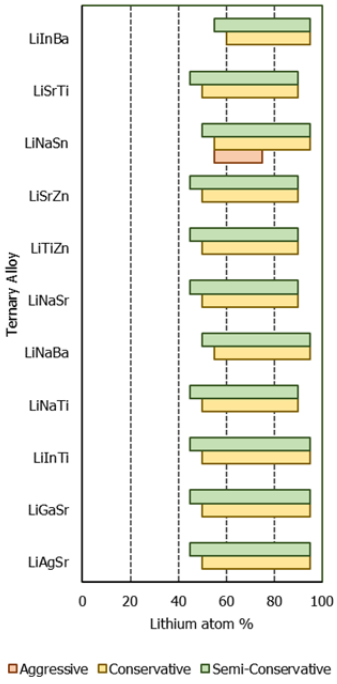
LiInBa
LiSrTi
LiNaSn
LiSrZn
LiTiZn
LiNaSr
LiNaBa
LiNaTi
LiInTi
LiGaSr
LiAgSr
Ternary Alloy
0
20
40
60
80
100
Lithium atom %
Aggressive
Conservative
Semi-Conservative

(c)

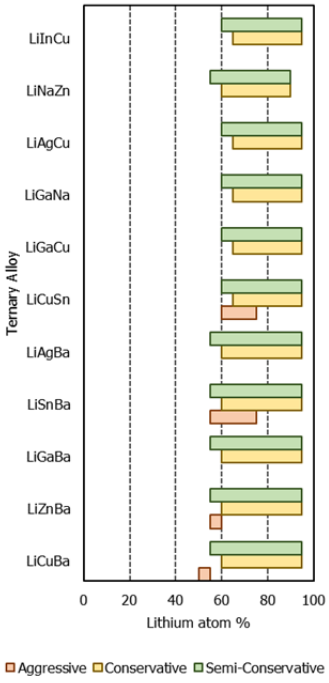
LiInCu
LiNaZn
LiAgCu
LiGaNa
LiGaCu
LiCuSn
LiAgBa
LiSnBa
LiGaBa
LiZnBa
LiCuBa
Ternary Alloy
0
20
40
60
80
100
Lithium atom %
Aggressive
Conservative
Semi-Conservative

(d)

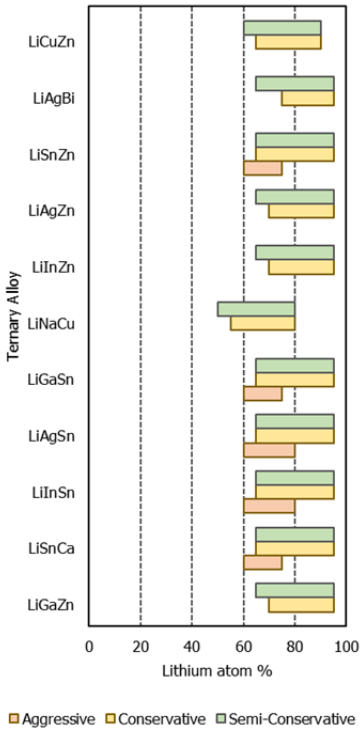

(e)

Figure 4: Range of lithium (atom %) for each ternary alloy that meet specific TBR and EMF criteria. Aggressive: TBR 1.02, EMF 1.2. Conservative: TBR 1.1, EMF 1.1. Semi-conservative: TBR 1.05, EMF 1.1. When an alloy does not meet one of the criteria at any composition, it is left blank.

All the alloys in Figure 4 meet both the conservative and semi-conservative criteria. The aggressive constrains are only met by alloys containing tin (and barium in one case) due to its high energy multiplication factor; all other cannot reach EMFs that are any higher than 1.15. As predicted, the conservative and semi-conservative constrains with the widest range of lithium concentrations were met by elements that performed well in the binary analysis such as barium, tin, and strontium, with lead or bismuth. Elements that have a combination of higher q-value and lower absorption cross section such as zinc will perform adequately when combined with high neutron multipliers such as lead, or elements with similar or better attributes, i.e. barium. Even gallium, whose absorption cross section is on the higher end but has above average q-value, yields satisfactory results with the elements formerly mentioned, specifically neutron multipliers. The ternaries in Figure 5 give a closer look at some of these alloys. Although the ranges that LiNaSn and LiSnZn meet limits are not as large as some of the other alloys, they do meet all three categories.

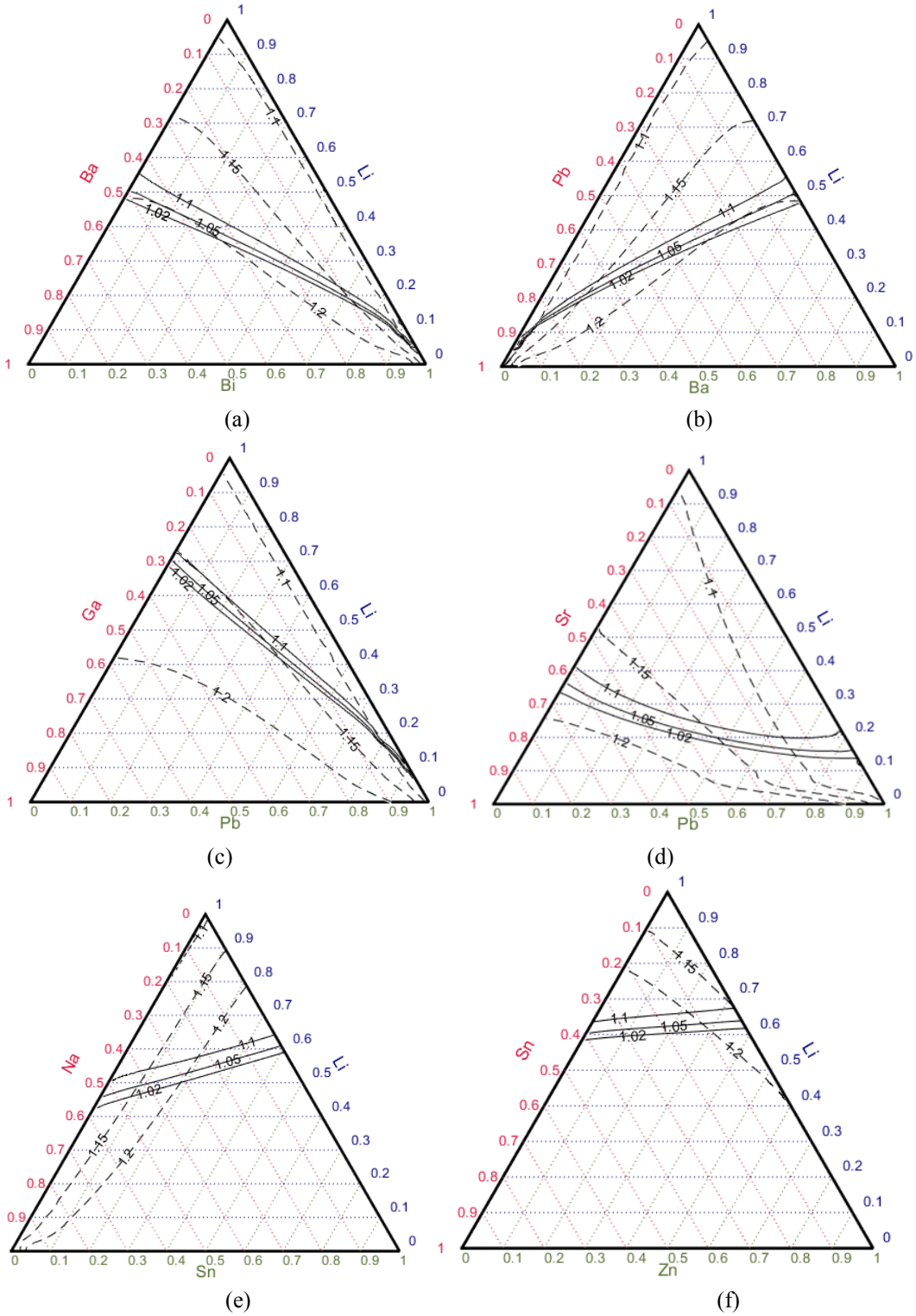

Figure 5: Ternary Plots for (a) LiBaBi, (b) LiPbZn, (c) LiGaPb, (d) LiSrPb, (e) LiNaSn, and (f) LiSnZn; solid lines represent TBR; dotted lines represent EMF.

The difference in lithium concentrations between each increase of TBR is not as significant as the change in EMF. Between TBRs of 1.02 and 1.1, respectively, the lithium concentration increases by less than 10%. This allows us to change the TBR constrains if necessary while still maintaining a similar minimum lithium concentration to reduce chemical reactivity. The increase of EMF from 1.1 to 1.2 is dependent on each individual alloy; smaller differences occur for alloys with higher q-values such as tin, zinc and gallium. Nevertheless, to increase the EMF for all alloys, the lithium concentration must be lowered by several percent for less absorption in the lithium and more absorption in the other components. As a result, all the alloys in Figure 5 other than tin, barely, if at all, meet any of the TBR limits with an EMF of 1.2.

3.3 Studies on Blanket Layers

A closer look at the contribution of tritium breeding in each layer of the blanket was examined and outlined in Table 4. This was done for LiSnZn at a composition of 65% lithium, 20% tin, and 15% zinc since it met all of the three criteria. Results show, as expected, that most of the breeding takes place in the middle layer, or layer 4 of the blanket. This is largely due to the fact that it is the largest of three layers, being 100 cm-thick. When observing tritium breeding in a per unit volume basis (last column in Table 4), it is shown that the innermost layer is the most effective as a result of high energy neutrons interacting with ^{7}Li. The outermost blanket layer will breed most of its tritium from low energy neutron reactions with ^{6}Li.

Table 3. Contributions to TBR from ^{6}Li and ^{7}Li in the three breeder/coolant layers.

Layer number	Volume m^3	Vol. Fraction (VF)	T6*	T7**	Layer TBR = T6+T7	TBR/VF
2	5.33	0.0053	0.0138	0.0089	0.0227	4.277
4	620.68	0.6167	0.7637	0.2254	0.9891	1.604
6	380.15	0.3778	0.0748	0.0018	0.0766	0.203
Total	1006.15	1	0.8523	0.2361	1.0883	1.088

*T6 = ^{6}Li(n,T) reactions per DT fusion
**T7 = ^{7}Li(n,n'T) reactions per DT fusion

Since the middle blanket layer produces the most tritium, a parametric study was conducted that varied the thickness of the layer from 20 cm to 200 cm by increments of 10 cm. Results for TBR and EMF are illustrated in Figure 6. The same trend is seen for TBR and EMF; when the thickness of the middle blanket layer is small, a lot of the neutrons will continue to travel to the outermost blanket layer where most of their interactions will take place. As the middle blanket layer thickness increases, the neutrons will have more interactions there and less will ever reach the outermost layer. Additionally, increasing the mid layer thickness reduces the probability of neutron leakage. This is prevalent by the slight increase in both TBR and EMF. Future work will examine changing the ratio of thicknesses between the middle layer and outer layer to examine how it affects TBR and EMF.

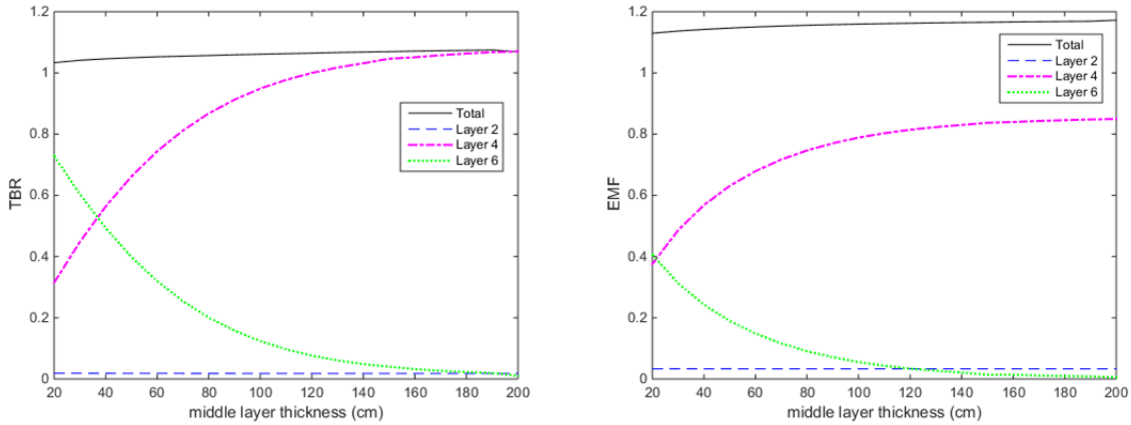

(a) (b)

Figure 6. TBR and EMF for varied middle blanket layer thickness.

3.3. Lithium enrichment

In order to further minimize the amount of lithium in the alloys and to increase TBR, the sensitivity to the concentration of lithium-6 was tested. The (n,t) cross section of ^{6}Li covers a wide range of energies as opposed to ^{7}Li, whose cross section only occurs in the high energy range; therefore, enriching the alloy in ^{6}Li increases neutron absorption in it and boosts TBR. LiSnZn was utilized for this enrichment sensitivity study. The chosen composition (65% Li, 20% Sn, 15% Zn) meets all three sets of criteria described in the previous Section. ^{6}Li's concentration was increased from natural (7.5%) to 90% with increments of 5%. Figure 7 shows that the EMF rapidly drops with increasing enrichment whereas TBR increases. The EMF exponentially decreases until 40% ^{6}Li, which is about where the TBR reaches its maximum. At such maximum (40%), the TBR is about 20% higher than with natural lithium. After this point the TBR becomes saturated and starts to slightly linearly decrease due to the lack of ^{7}Li(n,n'T) reactions. The ^{7}Li(n,n'T) reaction rate linearly decreases as a function of ^{6}Li enrichment, shown in Figure 7. Before 40% the ^{6}Li(n,T) reactions are increasing at a greater rate than ^{7}Li(n,n'T) reactions, overcoming them to allow the total TBR to increase. However, after 40%, the lack of additional neutrons from ^{7}Li(n,n'T) reactions prevent ^{6}Li from producing tritium at the same rate as it did with lower enrichments. This, plus the lack of tritium production from ^{7}Li causes the total TBR to decrease at enrichments greater than 40%. The (n,xn) reaction rate, influenced by tin, only slight decreases and does not have a strong influence on the behavior of the TBR.

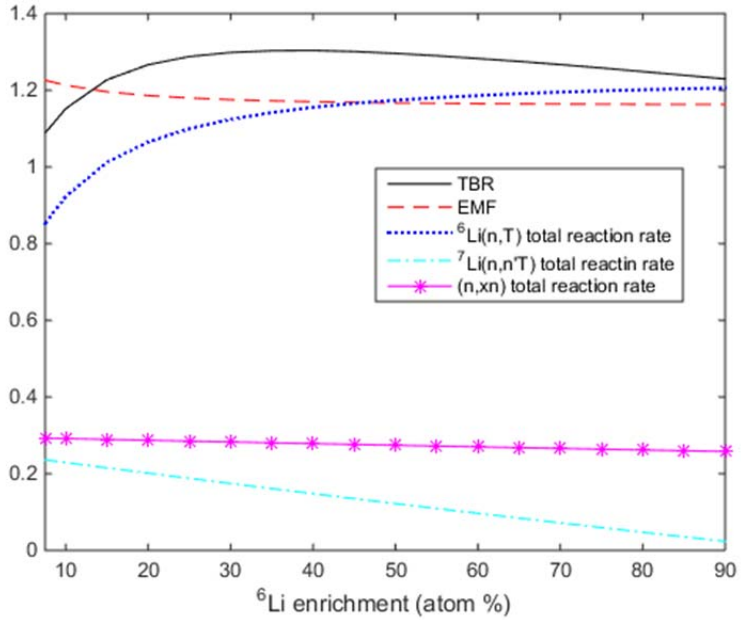

Figure 7. TBR,EMF, and (n,T) and (n,xn) reaction rates as a function of ^{6}Li concentration in lithium for Li(65%)Sn(20%)Zn(15%) alloy.

Figure 8 displays the range of total lithium concentrations in the LiSnZn alloy that meet each of the previously discussed criteria for three enrichment cases: natural, 40%, and 90%. The minimum lithium concentrations for each of the cases decrease as lithium enrichment increases. For example, the aggressive case decreases from 60 atom % for natural enriched lithium to 25 atom % for 40% enriched lithium. It decreases even further to 15 atom % total when lithium is enriched to 90%. Nevertheless, the case with 40% enriched lithium meets this criteria for a range of 35% of lithium concentrations (25 atom % to 60 atom % Li) as opposed to the 10% range in the case of 90% enrichment (15 atom % to 25 atom% Li). Additionally, the EMF is largely compromised as enrichment increases and thus, it is much harder for alloys of different concentrations in the 90% enriched case to meet the 1.2 EMF for the aggressive category. This is visualized in Figure 9 where ternary diagrams with ^{6}Li enriched at 40% and 90% are shown. It can also be seen in the ternaries how, for a constant lithium concentration, the TBR decreases when the amount of zinc in the alloy increases. This is due to the decrease of tin (n,xn) reactions, which lowers the neutron economy and reduces the number of Li(n,T) reactions. In addition, the phenomenon becomes more pronounced in the 90% enriched Li ternary due to the lack of ^{7}Li(n,n'T) reactions, which lowers the TBR as previously described. As a result, the TBR at 65% Li, 20% Sn, and 15% Zn will be lower (1.2) at 90% enriched lithium, than at 40%

(1.31). Minimizing the lithium concentration without lowering the energy multiplication factor and increasing the cost too much should be considered when selecting the lithium enrichment.

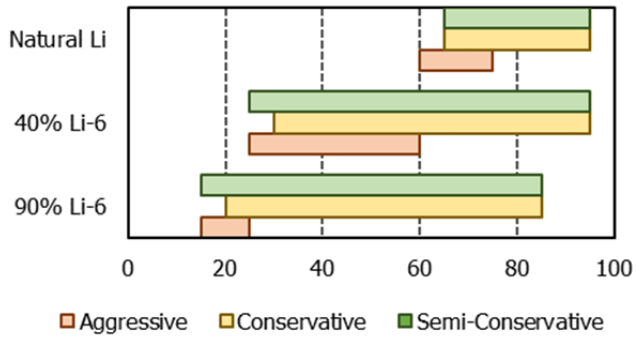

Figure 8. Range of lithium (atom%) for LiSnZn with natural, 40%, and 90% enrichment, that meet specific TBR and EMF criteria. Aggressive: TBR 1.02, EMF 1.2. Conservative: TBR 1.1, EMF 1.1. Semi-conservative: TBR 1.05, EMF 1.1.

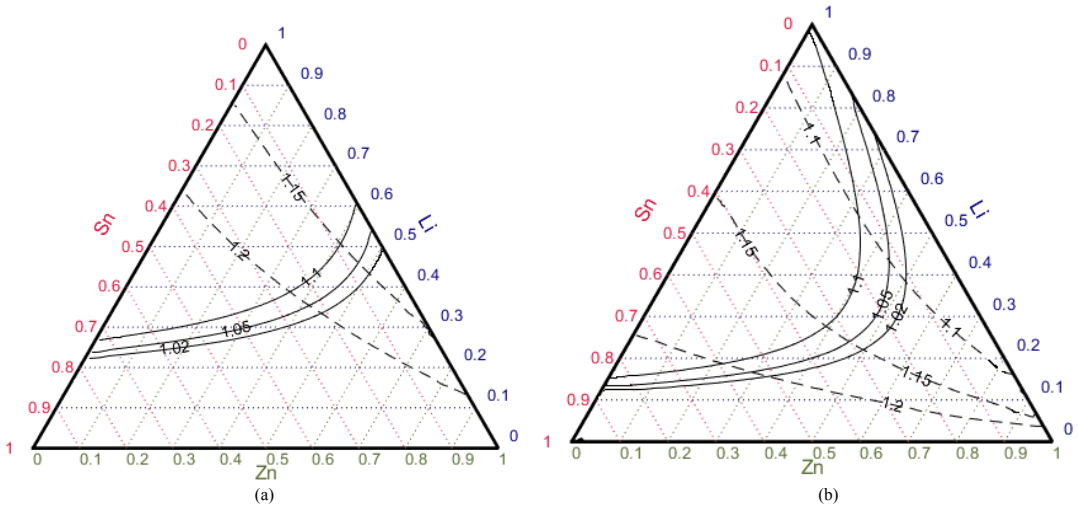

Figure 9. Ternary diagrams for LiSnZn with lithium enriched to (a) 40% and (b) 90%; the solid lines represent TBR; dotted lines represent EMF.

3.4. Activation Analysis

Eight alloys were chosen for an extensive activation analysis: LiBaBi, LiPbBa, LiSnZn, LiCuPb, LiGaPb, LiSrPb, LiPbZn, and LiNaSn. These alloys were chosen based on their neutronic performance: alloys with lead and bismuth exhibit high neutron multiplication and minimize the amount of lithium in the alloy; alloys with tin meet all of the three sets of criteria in the previous analysis. The composition for each alloy (Table 4) was selected to meet the conservative or semi-conservative set of criteria while minimizing the amount of lithium. These are all with natural lithium.

Table 4: Compositions of Alloys Chosen for Activation Analysis

Alloy	Composition (%)
LiBaBi	20-10-70
LiPbBa	25-60-15
LiSnZn	65-20-15

LiCuPb	40-20-40
LiGaPb	50-10-40
LiSrPb	30-50-20
LiPbZn	30-60-10
LiNaSn	55-30-15

Results for the parameters described in Section 2.3 are analyzed in the following paragraphs.

Decay heat

The decay heat is plotted in Figure 10. LiPbBa is the alloy with the lowest decay heat and the only one that can utilize dry cooling right after shutdown. Most of the decay heat in this alloy stems from ^{137m}Ba, ^{137}Cs, and ^{133}Ba. On the contrary, LiBaBi exhibits the highest decay heat due to ^{210}Po, a decay product of ^{210}Bi shown in Figure 11(a). The decay heat remains high in this alloy after one and a half years when polonium decays due to contributions from ^{207}Bi and ^{208}Bi. During the first year and a half LiBaBi must be wet cooled; afterwards, dry cooling can be utilized. Alloys containing tin and zinc behave fairly similar; LiPbZn and LiSnZn have the greatest contribution from ^{65}Zn. After one year the activation products of tin do not allow the two tin-containing alloys to decay at the same rate as LiPbZn. Nevertheless, all three of the alloys can be switched from wet cooling to dry after one year. Other lead containing alloys such as LiSrPb and LiCuPb decay at faster rates such that dry cooling can be implemented for LiSrPb in less than a month, and for LiCuPb in less than a week. LiGaPb is an interesting case—^{72}Ga causes the decay heat of LiGaPb to be large in the beginning as seen in Figure 11(a). However, it significantly decreases after one week and becomes the alloy with the lowest decay heat. At this time LiGaPb will not need any additional active cooling. Most of the other alloys will not need active cooling after 100 years with the exception of LiSrPb and LiPbZn who meet this constrain of 10 W/m^3 only after 10 years, and LiBaBi, who does not meet this limit within the 300 years examined.

Contact dose rate

Contact dose rates for all the alloys are illustrated in Figure 12. Similarly to the decay heat, LiGaPb has the highest contact dose rate for the first week until ^{72}Ga decays, shown in Figure 13(a). After this time, hypothetically speaking, it would be possible to remotely move a container with the entire volume of the LiGaPb blanket. Once the gallium alloy decreases, alloys with zinc portray the largest contact dose rates from contributions of ^{65}Zn (Figure 13(a)). LiNaSn is also in the same range of contact dose rates at the beginning before ^{24}Na and ^{22}Na decay, shown in Figure (13(b)). Lead containing alloys such as LiPbZn, LiSrPb, and LiPbBa, portray the lowest contact dose rates for the first six months. By this time, the contact dose rate of LiSrPb has significantly decreased due to the decay of ^{85}Sr. On the contrary, the decay of LiPbBa occurs much more slowly and LiPbZn decays much later, after five years. At this point the contact dose rates of the other alloys are much lower. The one exception is LiBaBi, whose isotopes decay at the slowest rate of any other alloy, only decreasing the contact dose rate by an order of a magnitude and a half in the first 300 years. Every alloy except LiPbBa, and LiBaBi will be able to be remotely handled with the entire blanket volume at 100 years. By 300 years, the only alloy that will not meet the 10 mSv/h constrain with 100% of its volume is LiBaBi.

Accident dose

Unlike decay heat and contact dose rates, results for accident dose include the contribution of tritium. Tritium will be separated from the rest of the coolant after shutdown and recycled. Whereas decay heat and contact dose rates are measured after shutdown, a loss of coolant or flow is most likely to occur during normal operation. The accident scenario in this study assumes immediate release of the coolant to the environment without the use of any shielding or containment structure to stop the release. Additionally, it is important to note that results for accident doses, shown in Table 5, are conservative due to the use of the Piet release fractions as opposed to release fractions modeled from real accident scenarios. From the results, ^{210}Po (decay product of ^{210}Bi) contains a high DCF and causes the accident dose to be the highest in LiBaBi. Alloys containing lead such as LiPbBa and LiPbZn will also be compromised by ^{210}Po. Nevertheless, direct production of polonium from bismuth causes the accident dose to be at least three orders of magnitude higher. The accident dose in zinc containing alloys will be dominated by ^{65}Zn due to its high radioactivity and release fraction. The lowest accident doses are from LiPbBa and LiSrPb, being only half of

what it is for LiCuPb. With the exclusion of LiBaBi, the accident dose constraint will only be met for all the alloys if about 50-200 cm^3 of coolant escapes.

Waste disposal rating

The last activation parameter accounted for was the WDR to verify that alloys meet requirements for shallow land burial. These are listed in Table 5 for the entirety blanket volume. All the alloys meet the WDR criteria (<1) except for LiBaBi; this is due to ^{208}Bi.

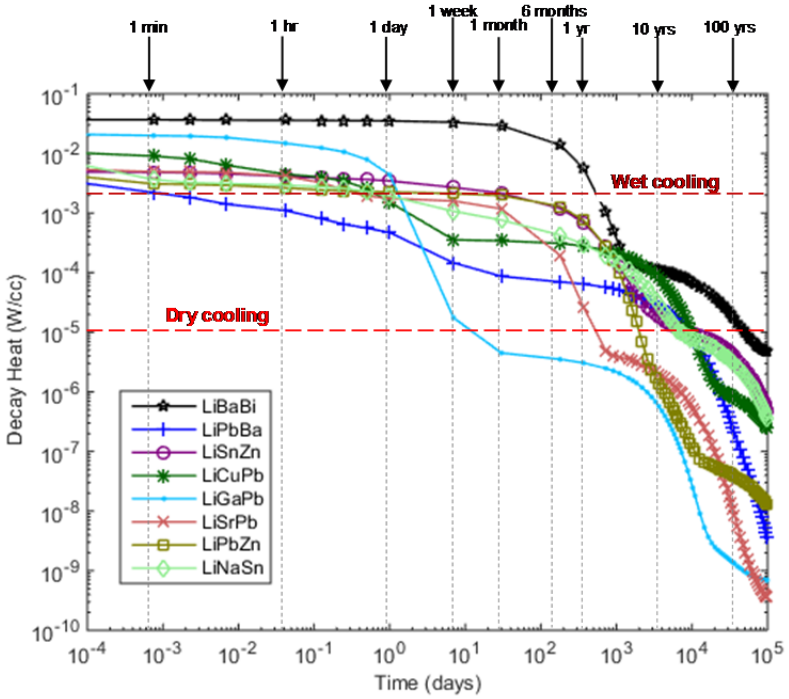

Figure 10. Decay heat (W/cm^3) as a function of time after irradiation for breeder/coolant ternary alloys. The wet cooling and dry cooling constrains are indicated by the horizontal lines.

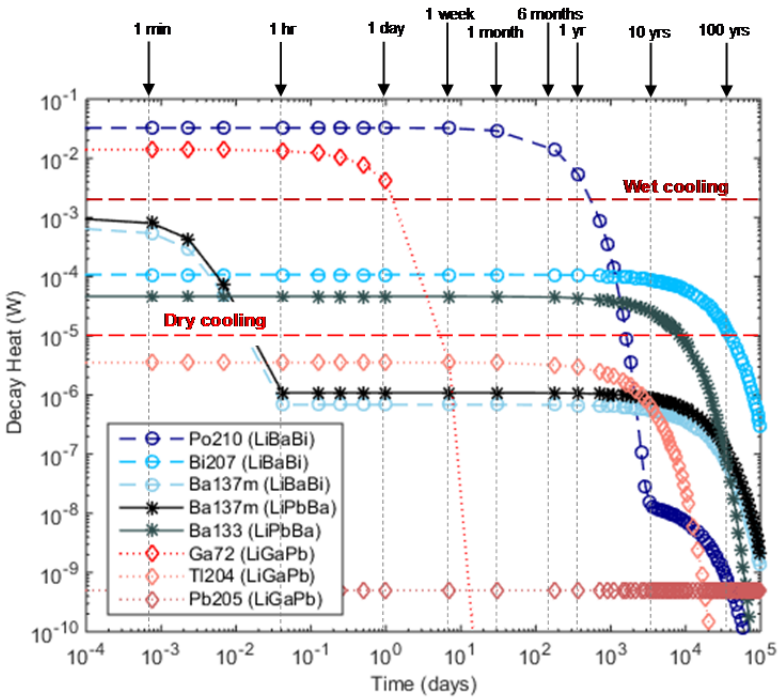

(a)

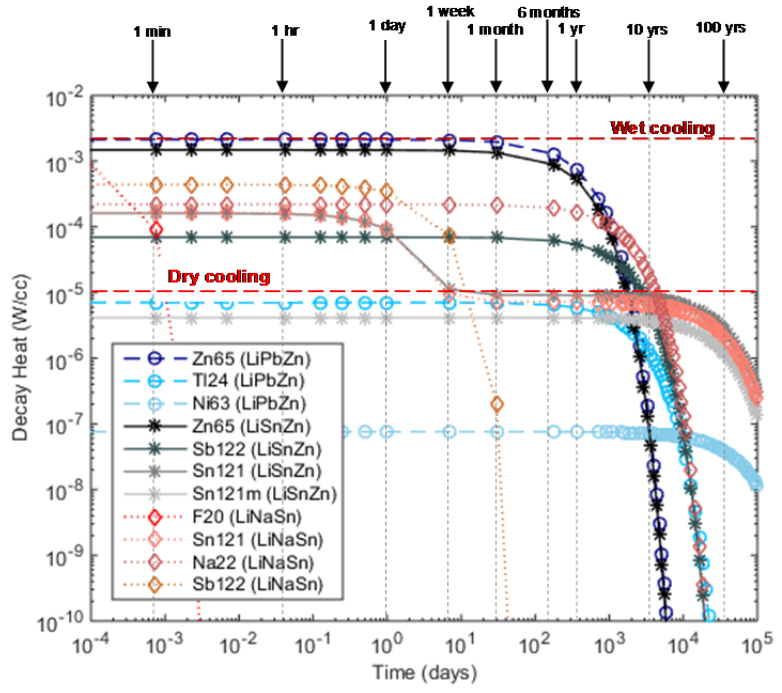

(b)

Figure 11. Isotopics of decay heat (W/cm^3) after irradiation for (a) LiBaBi, LiPbBa, and LiGaPb and (b) LiPbZn, LiSnZn, and LiNaSn. The wet cooling and dry cooling constrains are indicated by the horizontal lines.

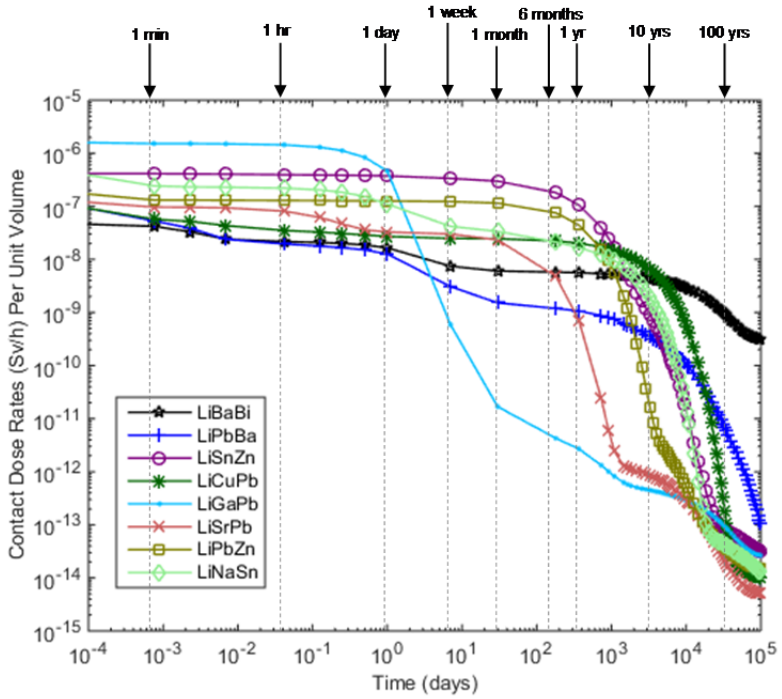

Figure 12. Contact Dose Rates (Sv/h) as a function of time after irradiation for breeder/coolant ternary alloys.

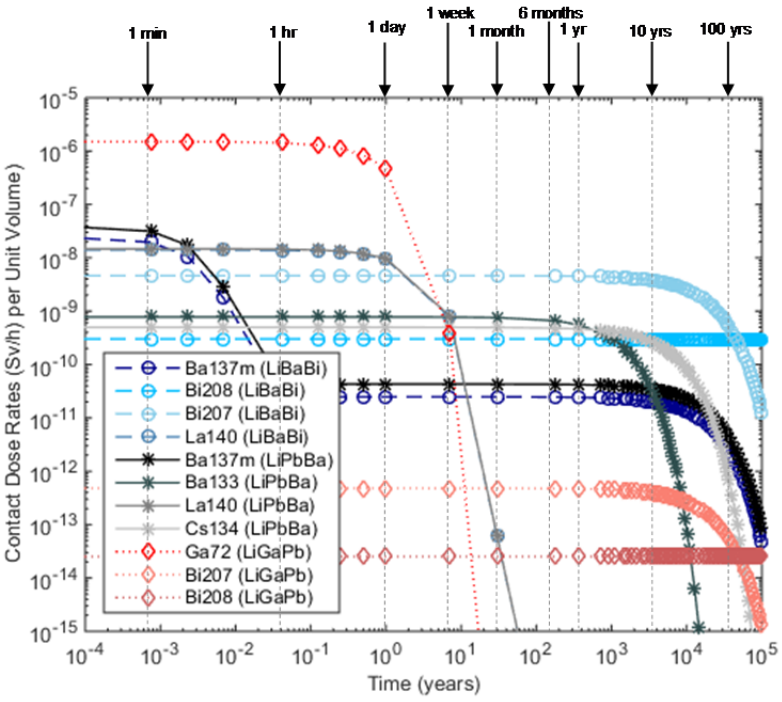

(a)

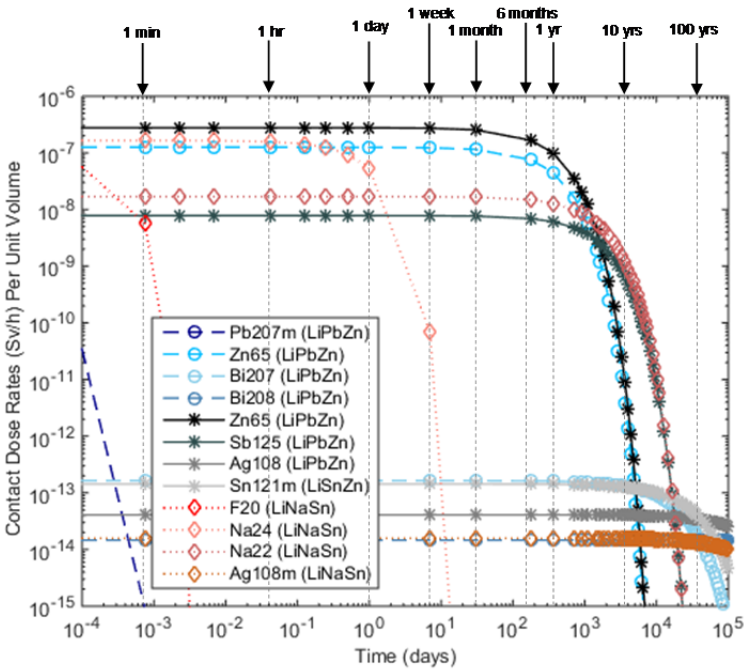

(b)

Figure 13. Isotopics of Contact Dose Rates (Sv/h) for (a) LiBaBi, LiPbBa, and LiGaPb and (b) LiPbZn, LiSnZn, and LiNaSn.

Table 5. Accident Dose (AD) and Waste Disposal Ratings (WDR) for alloys.

Alloy	**AD (mSv/cm^3)**	**WDR**
LiBaBi	154.05	3410
LiPbBa	0.0564	0.19
LiSnZn	0.1082	0.09
LiSrPb	0.0577	0.05
LiGaPb	0.1003	0.18
LiCuPb	0.1171	0.15
LiPbZn	0.1246	0.2
LiNaSn	0.0662	0.07

From the evaluation above, LiBaBi exhibited the poorest performance from all the alloys, mainly due to bismuth. Additionally, the high amounts of polonium generated from bismuth alloys can be of concern due to its toxic and poisonous qualities [28-29]. With its high release fraction, it can easily travel and be ingested by the public. As a result of all this, bismuth-containing alloys will not be considered as potential candidates for the coolant/breeder. Although ^{72}Ga had a short life, it was still the major isotope that exhibited high decay heat, accident dose, and contact dose, respectively, and should be utilized with caution. In addition, ^{60}Co, an activation product of zinc, can also be chemically toxic [30]. Although LiSrPb and LiCuPb were not closely examined in this study, they seemed to perform fairly well compared to other alloys specially those containing tin and zinc. Future work will take a closer look at the activation of strontium and copper.

4. Conclusions

The Lawrence Livermore National Laboratory is investigating the possibility to design lithium ternary alloys to replace lithium as blanket breeder/coolant for the Laser Inertial Fusion Energy power plant that have similar breeding, corrosion, and thermal properties, but reduced chemical reactivity as compared to lithium. This study performed neutronic and activation analysis of numerous lithium ternary alloys in order to assess their performance in an IFE blanket and guide the down selection process. The neutronic analysis determined energy multiplication factor and tritium breeding ratio. It was found that the best performing alloys (higher TBR and higher EMF) combine elements that exhibit low absorption cross section and high q-value such as tin, barium, strontium, and zinc, with elements with high neutron multiplying cross sections, like lead and bismuth. A large number of alloys, especially with combinations formerly described, met TBR constrains of 1.05 and 1.1 and an EMF constrain of 1.1 for a wide range of lithium concentrations. When the EMF constraint was increased to 1.2, the demand to produce additional power was too high for most alloys except for those containing tin. Additionally, it was found that when an alloy already contains a high amount of lithium (greater than 50%), doubling the ^{6}Li content in lithium from 7.5% to 15% increases TBR by 13%. After a certain percent of enriched ^{6}Li, the lack of tritium and additional neutrons produced from ^{7}Li(n,n'T) reactions ends up reducing the TBR. At lower total lithium concentrations (<50%), the TBR will continue to increase to higher ^{6}Li enrichments since the ^{7}Li(n,n'T) reactions will not be as significant.
Activation calculations were performed for a series of elements that exhibited good TBR and EMF properties. This analysis revealed bismuth as a poor choice; it had the highest numbers for all of the criteria evaluated. Alloys containing zinc and tin also showed some of the highest decay heats, contact dose rates, and accident doses. Most of the alloys examined can be stored in dry containers at an estimated one year after shutdown. Additionally, if necessary, the entire volume of the blanket for every alloy except LiPbBa and LiBaBi could be remotely handled. Accident doses were high in alloys containing zinc, copper, or gallium, but were not high enough to pose a major safety concern. With the exception of LiBaBi, activation analysis demonstrated that all the alloys could be utilized as blankets of the IFE reactor without posing major environmental or safety concerns.
Future work will look further to examine activation in additional alloys to see how the elements compare to those reviewed in this work. Possibility of lithium enrichment will also be considered.

Acknowledgements

The authors would like to thank Dr. Kevin Kramer, now with TerraPower, for his guidance early in this project. This work was support by LLNL LDRD Project 14-ERD-035. Portions of this work were performed under the auspices of the U.S. Department of Energy by Lawrence Livermore National Laboratory under Contract DE-AC52-07NA27344.

References

[1] J. F. LATKOWSKI, et al., "Chamber Design for the Laser Inertial Fusion Energy (LIFE) Engine," *Fusion Sci. Technol.,* **60**, 54-60 (2011).

[2] M.L. CORRADINI, D.W. JEPPSON. "Lithium Alloy Chemical Reactivity with Reactor Materials: Current State of Knowledge." *Fusion Engineering and Design* 14.3-4, 273-88 (1991).

[3] T. IHILI, et al., "Review of Blanket Designs for Advanced Fusion Reactors." *Fusion Engineering and Design* 83.7-9, 912-19 (2008).

[4] ABDOU, M. A. "Overview of Fusion Blanket R&D in the US Over the Last Decade." *Nuclear Engineering and Technology* 37.5, 401-22 (2005).

[5] T.K. GIL, M.S. KAZIMI, "The Kinetics of Liquid Lithium Reaction with Oxygen/Nitrogen Mixtures," MIT PFC/RR-83-1 (1986).

[6] N.B. MORLEY, et al., "Recent Research and Development for the Dual-Coolant Blanket Concept in the US," *Fusion Engineering and Design*, **83**, 920-927 (2008).

[7] E. I. MOSES, "The National Ignition Facility and the Promise of Inertial Fusion Energy," *Fusion Sci. Technol.*, **60**, 11-16 (2011).

[8] M. DUNNE, et al., “Timely Delivery of Laser Inertial Fusion Energy (LIFE),” *Fusion Sci. Technol.*, **60**, 19-27 (2011).
[9] R. SACKS, et al., “Parameter Study of an Inertial Fusion Energy Chamber Response Using the 1-D Bucky Radiation Hydrodynamics Code.” *Fusion Sci Technol.,* **66**, 349-57 (2014).

[10] W.R. Meier, “Fusion Power Multiplication for LIFE,” LLNL Report LLNL-MI-666819 (Feb. 3, 2015).

[11] T. GOORLEY et al., ‘‘Initial MCNP6 Release Overview,’’ Nucl. Technol., 180, 3, 298 (2012); http://dx.doi.org/10.13182/NT11-135.

[12] M.B. CHADWICK, et al., ENDF/B-VII.0: Next Generation Evaluated Nuclear Data Library for Nuclear Science and Technology. Nuclear Data Sheets, **107** 2006 2931-3060.

[13] W. Meier, P. Amendt, Personal communication, 2014.

[14] L.A. EL-GUEBALY, S. MALANG. “Toward the Ultimate Goal of Tritium Self-sufficiency: Technical Issues and Requirements Imposed on ARIES Advanced Power Plants.” *Fusion Engineering and Design*, **84**, 2072-83 (2009).

[15] S. REYES, et al., “LIFE Tritium Processing: A Sustainable Solution for Closing the Fusion Fuel Cycle.” *Fusion*
Sci. Technol., **64**, 187-93 (2013).

[16] W.R. MEIER, E.C. MORSE. “Blanket Optimization Studies for the HYLIFE Inertial Confinement Fusion Reactor.” *Fusion Technology*, **8**, 2681-95 (1985).

[17] J. SANZ, O. CABELLOS, N. GARCIA-HERRANZ. “ACAB. Inventory Code for Nuclear Applications: User’s Manual V.2008.” Madrid, Spain (2008).

[18] R.A. FORREST, The European Activation System: EASY-2007 Overview, UKAEA FUS 533, 2007

[19] S.M. QAIM. *Nuclear Data for Science and Technology: Proceedings of an International Conference Held at the Forschungszentrum Jülich, Fed. Rep. of Germany, 13-17 May 1991*. Berlin: Springer-Verlag, 860-62 (1992).

[20] J.P. CATALAN, F. OGANDO, J. SANZ, “Activation Analysis for a He/LiPb Dual Coolant Blanket for DEMO Reactor,” Fusion Sci. Technol., 60, 438-442 (2011).

[21] S D.A. PETTI, et al., “Re-evaluation of the Use of Low Activation Materials in Waste Management Strategies for Fusion,” Fusion Engineering and Design, 51-52, 435-444 (2000).

[22] S.J. PIET, E.T. CHENG, and S. HERRING, "Initial Integration of Accident Safety Waste Management, Recycling, Effluent, and Maintenance Considerations for Low-Activation Materials," Fusion Technology, 19, 146-61 (1989).

[23] J.F. LATKOWSKI, J. SANZ, S. REYES, J. GOMZ DEL RIO, “Selection of IFE Target Materials from a Safety and Environmental Perspective,” Nuclear Instruments and Methods in Physics Research, A 464, 422-427 (2001).

[24] D. LAYCAK, “Preliminary Study of Radiological Doses from Released Nuclides from LIFE Reactor,” LLNL Safety Division, May 2012.

[25] S.J. PIET, E.T. CHENG, and L.J. PORTER, "Accident Safety Comparison of Elements to Define Low-Activation Materials," Fusion Technology, 17, 636-57 (1990).

[26] P.E Turchi, "Thermodynamic Assessment of the Ternary Alloy System Li-Sn-Zn, " LLNL report LLNL-TR-653675, April 2014.

[27] S. MALANG, R. MATTAS. “Comparison of Lithium and Eutectic Lead-lithium Alloy, Two Candidate Liquid Metal Breeder Materials for Self-Cooled Blankets.” *Fusion Engineering and Design*, **27**, 399-406 (1995).

[28] J. Harrison, et al., “Polonium-210 as a Poison.” *Journal of Radiological Protection*, **27**, 17-40 (2007).

[29] G.I. Khorasanov, A.P. Ivanov, and A.I. Blokhin. “Polonium Issue in Fast Reactor Lead Coolants and One of the Ways of Its Solution.” *Proceedings from ICONE10 10th International Conference on Nuclear Engineering*. (2002).

[30] L. R. Payne. “The Hazards of Cobalt.” *Occupational Medicine*, **27**, 20-25 (1977).

Appendix A – Binary plots

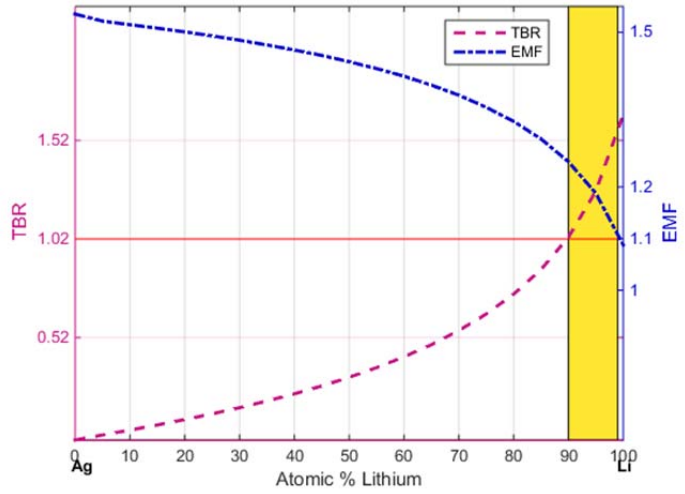

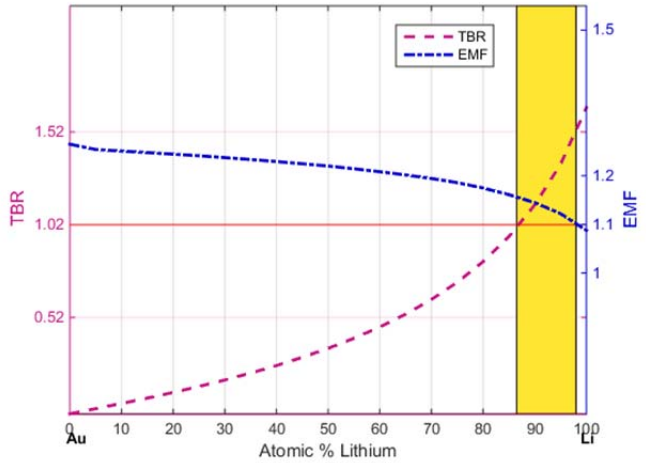

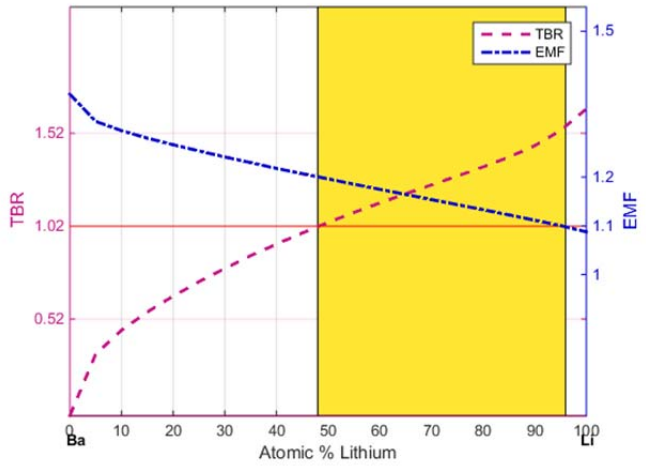
TBR
EMF
1.52
1.02
0.52
1.5
1.2
1.1
1
0
10
20
30
40
50
60
70
80
90
100
Ba
Li
Atomic % Lithium

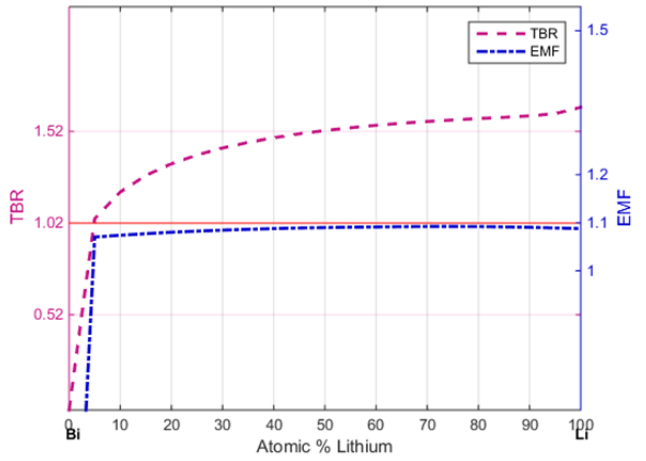
TBR
EMF
1.52
1.02
0.52
1.5
1.2
1.1
1
0
10
20
30
40
50
60
70
80
90
100
Bi
Li
Atomic % Lithium

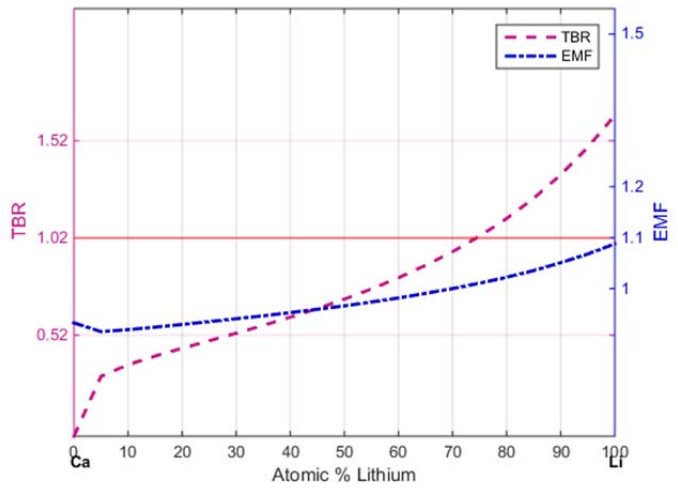
TBR
EMF
1.52
1.02
0.52
1.5
1.2
1.1
1
0
10
20
30
40
50
60
70
80
90
100
Ca
Li
Atomic % Lithium

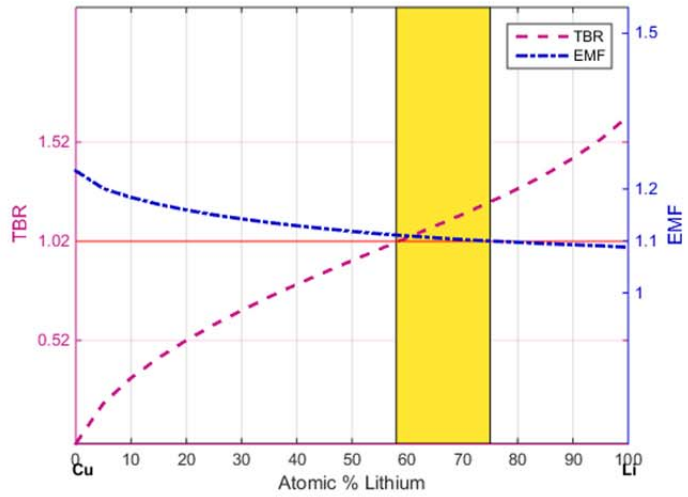
TBR
EMF
1.52
1.02
0.52
1.5
1.2
1.1
1
0
10
20
30
40
50
60
70
80
90
100
Cu
Li
Atomic % Lithium

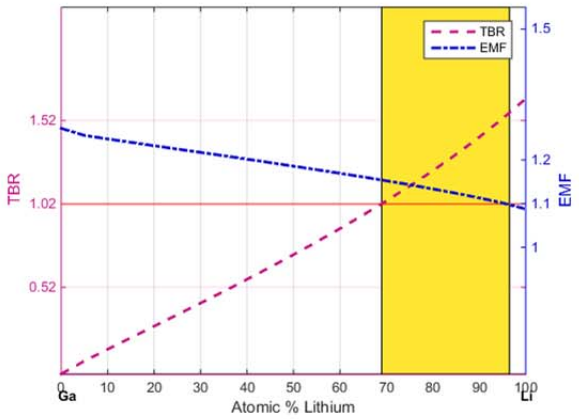
TBR
EMF
1.52
1.02
0.52
1.5
1.2
1.1
1
0
10
20
30
40
50
60
70
80
90
100
Ga
Li
Atomic % Lithium

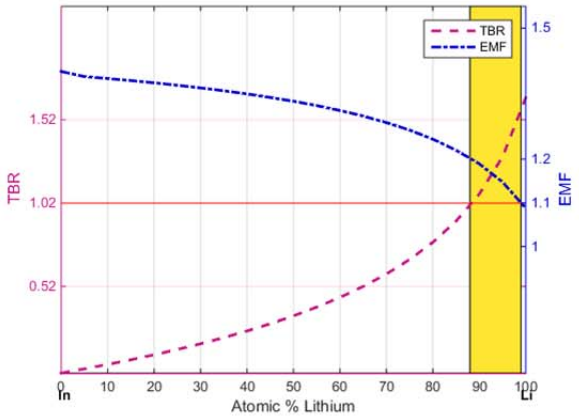
TBR
EMF
1.52
1.02
0.52
1.5
1.2
1.1
1
0
10
20
30
40
50
60
70
80
90
100
In
Li
Atomic % Lithium

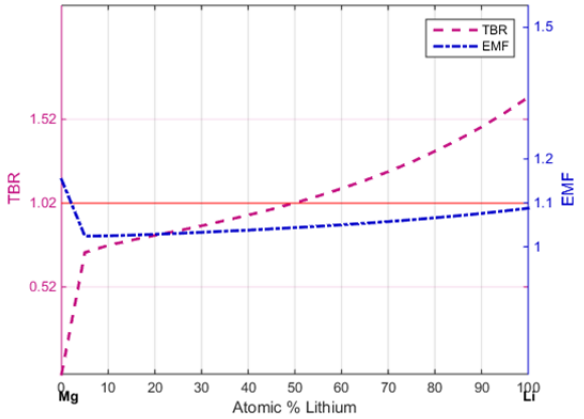
TBR
EMF
1.52
1.02
0.52
1.5
1.2
1.1
1
0
10
20
30
40
50
60
70
80
90
100
Mg
Li
Atomic % Lithium

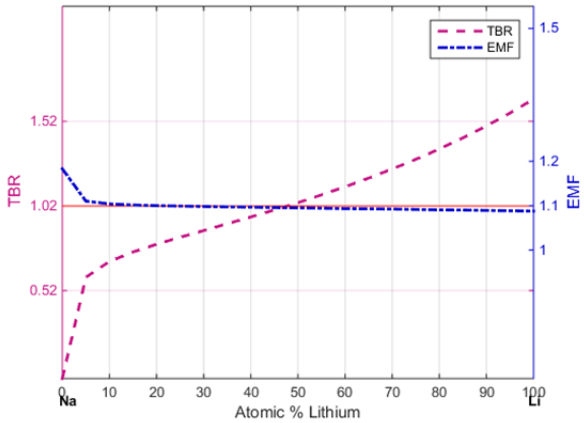
TBR
EMF
1.52
1.02
0.52
1.5
1.2
1.1
1
0
10
20
30
40
50
60
70
80
90
100
Na
Li
Atomic % Lithium

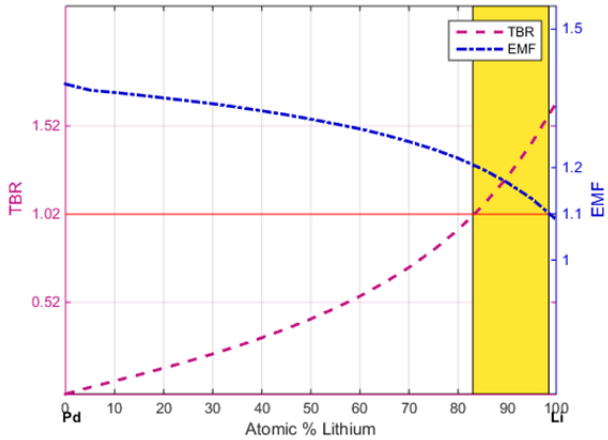
TBR
EMF
1.52
1.02
0.52
1.5
1.2
1.1
1
0
10
20
30
40
50
60
70
80
90
100
Pd
Li
Atomic % Lithium

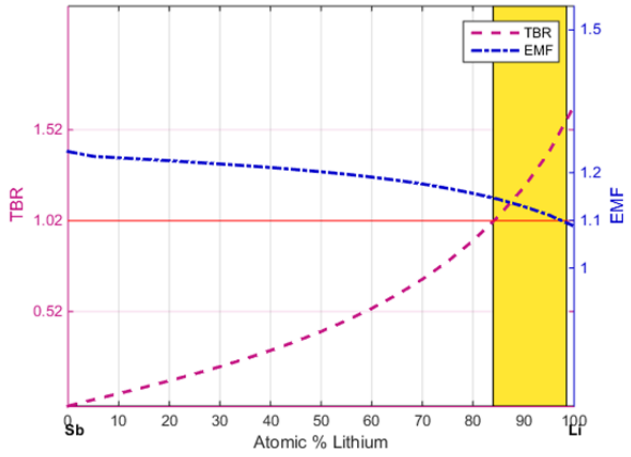
TBR
EMF
1.52
1.02
0.52
1.5
1.2
1.1
1
0
10
20
30
40
50
60
70
80
90
100
Sb
Li
Atomic % Lithium

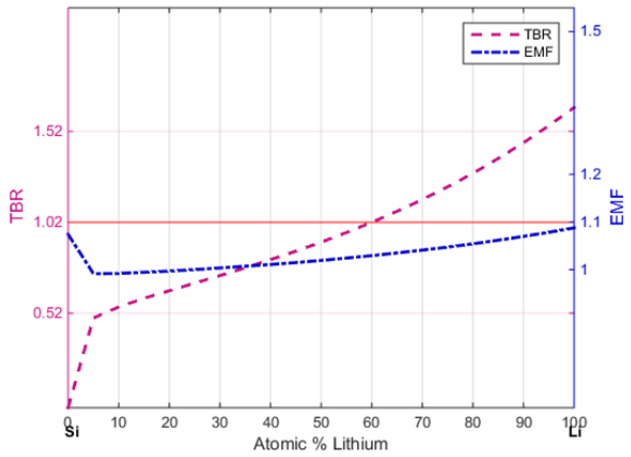
TBR
EMF
1.52
1.02
0.52
1.5
1.2
1.1
1
0
10
20
30
40
50
60
70
80
90
100
Si
Li
Atomic % Lithium

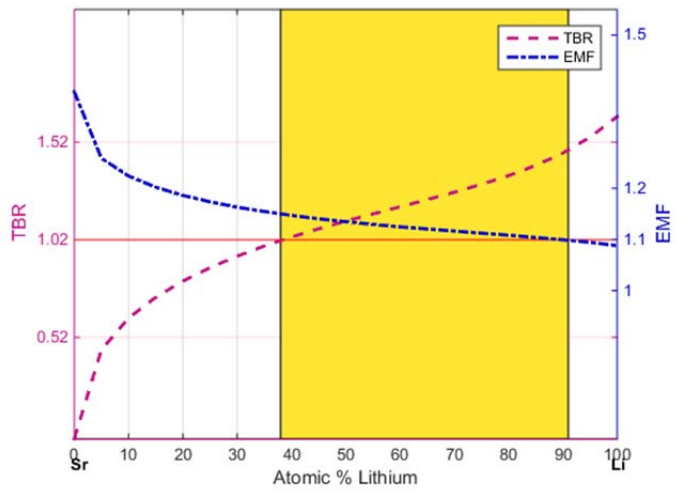
TBR
EMF
1.52
1.02
0.52
1.5
1.2
1.1
1
0
10
20
30
40
50
60
70
80
90
100
Sr
Li
Atomic % Lithium

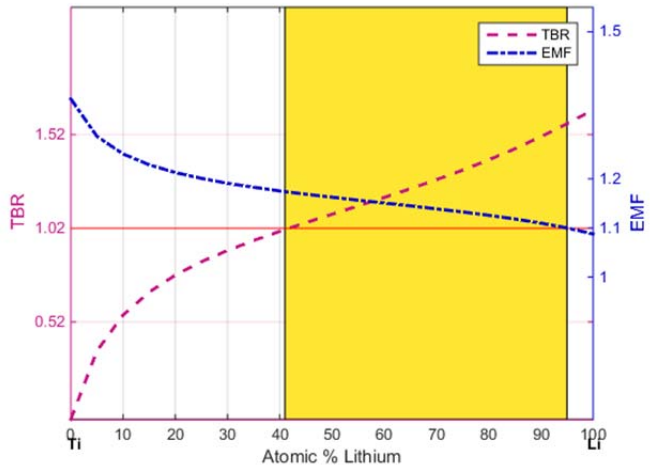

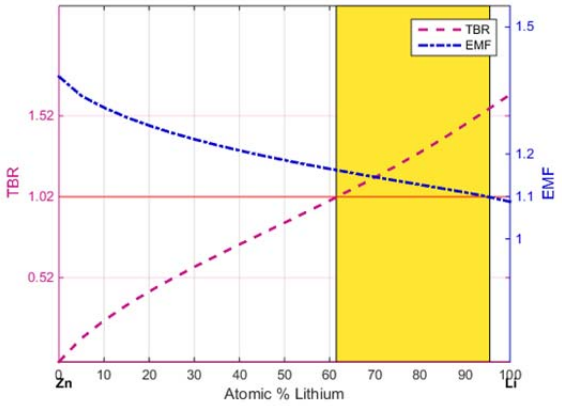

Appendix B – Ternary plots
On the left: TBR with the three chosen constraints
On the right: EMF with the three chosen constraints

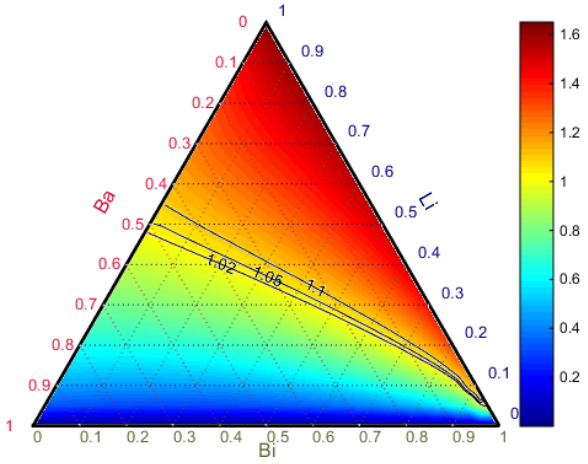

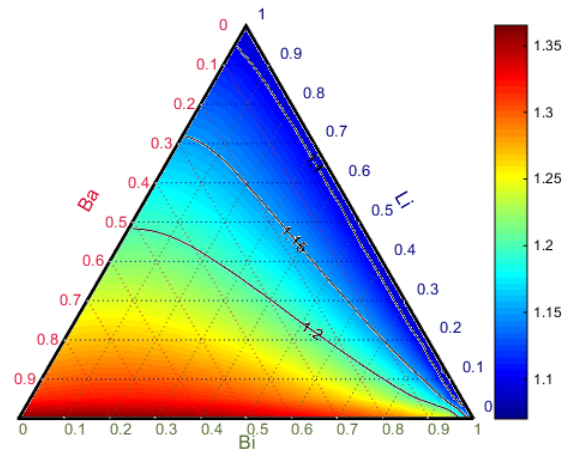

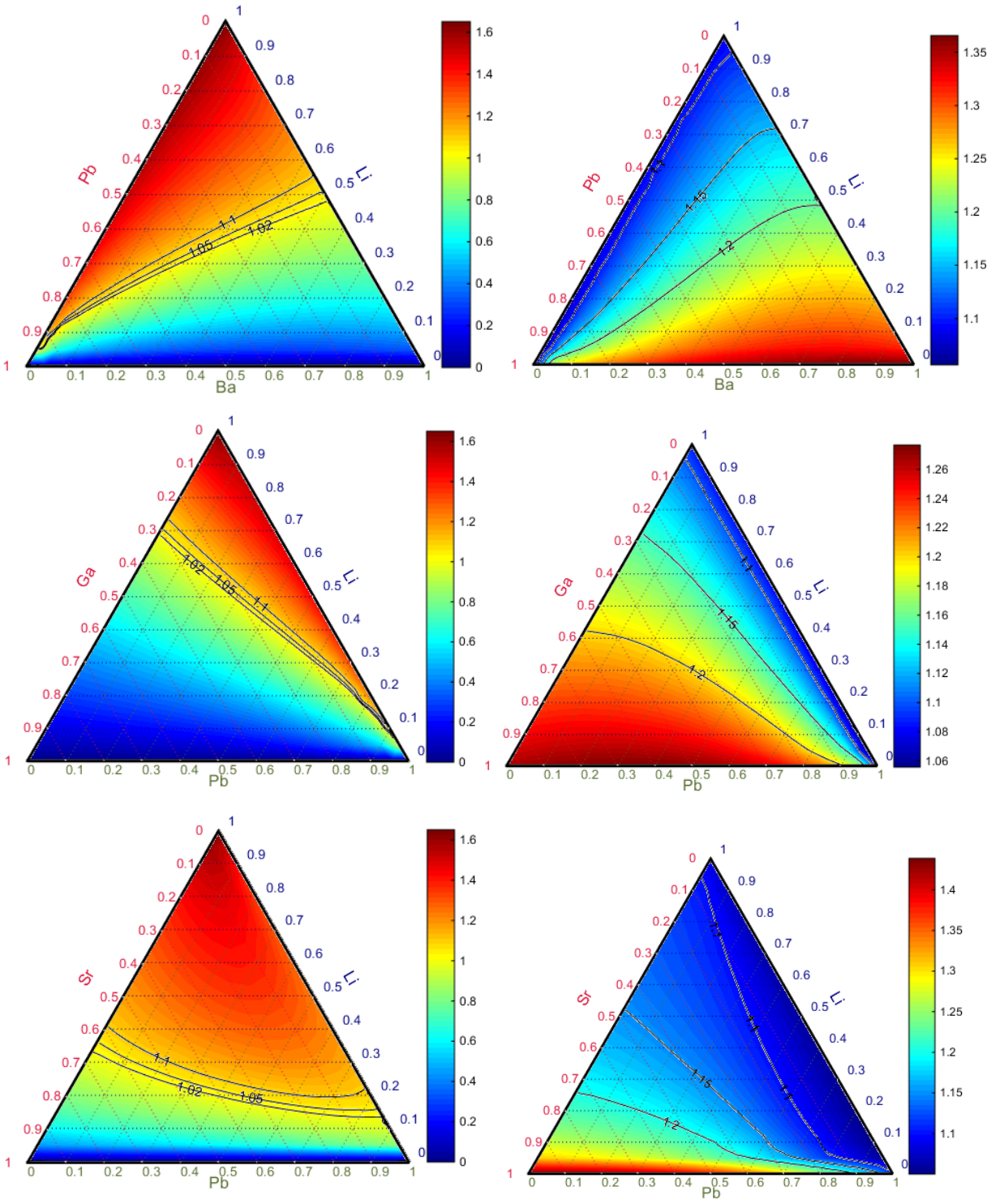
Pb
Ba
Cl
1.02
1.05
1.1
1.15
1.2
Ga
Pb
Cl
1.02
1.05
1.1
1.15
1.2
Sr
Pb
Cl
1.02
1.05
1.1
1.15
1.2

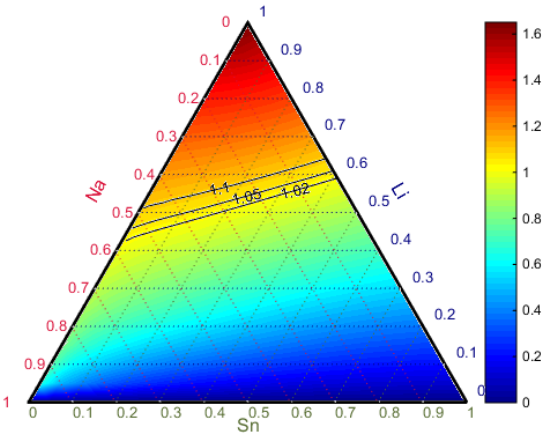
Na
Li
Sn
1.1
1.05
1.02

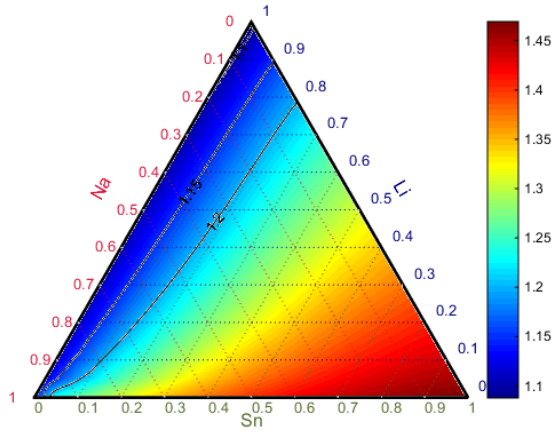
Na
Li
Sn
1.15
1.2

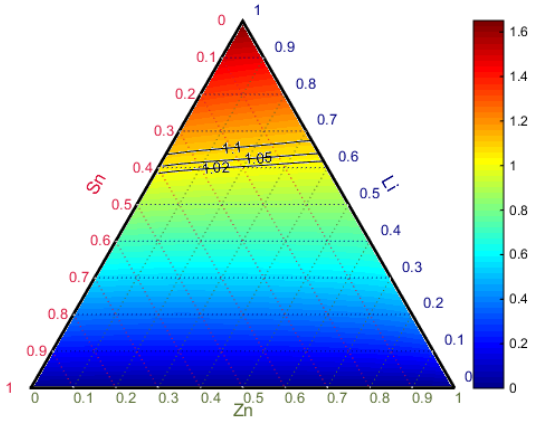
Sn
Li
Zn
1.1
1.05
1.02

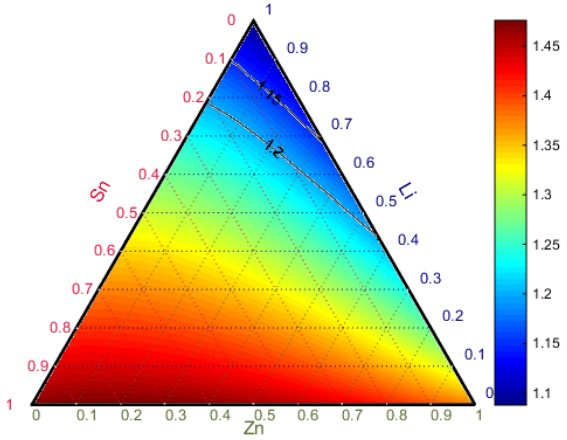
Sn
Li
Zn
1.15
1.2

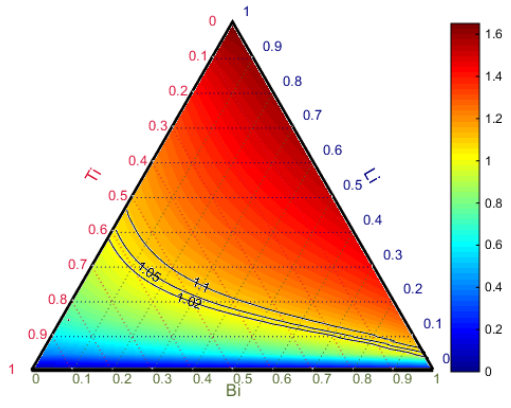
Ti
Li
Bi
1.05
1.1
1.02

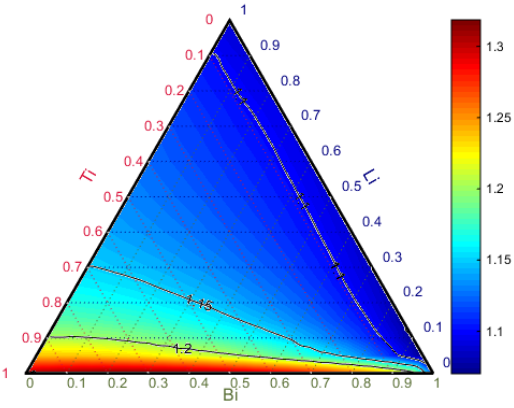
Ti
Li
Bi
1.15
1.2

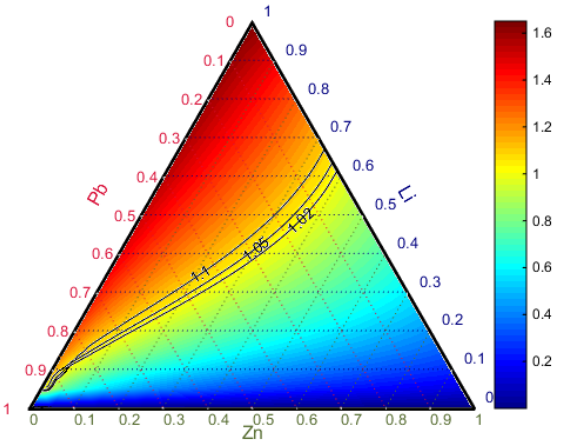
Pb
Li
Zn
1.1
1.05
1.02
1.6
1.4
1.2
1
0.8
0.6
0.4
0.2

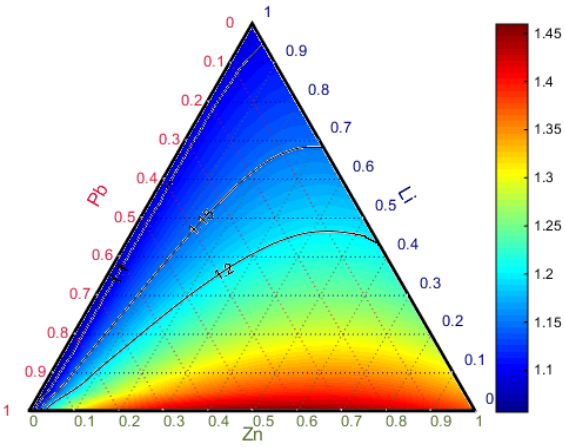
Pb
Li
Zn
1.15
1.2
1.45
1.4
1.35
1.3
1.25
1.2
1.15
1.1

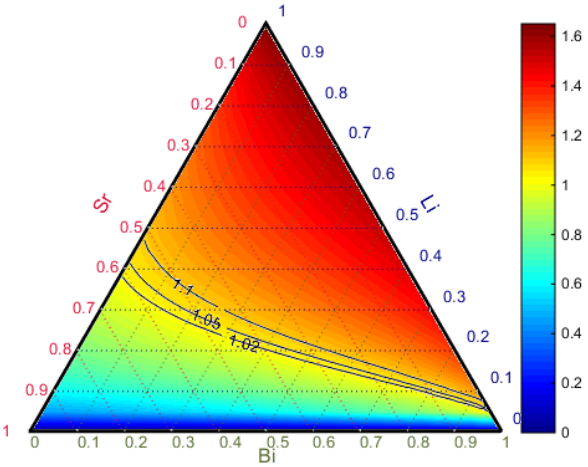
Sr
Li
Bi
1.1
1.05
1.02
1.6
1.4
1.2
1
0.8
0.6
0.4
0.2

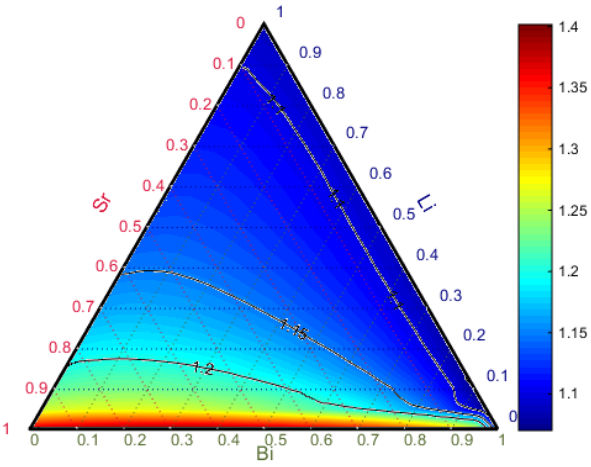
Sr
Li
Bi
1.05
1.2
1.4
1.35
1.3
1.25
1.2
1.15
1.1

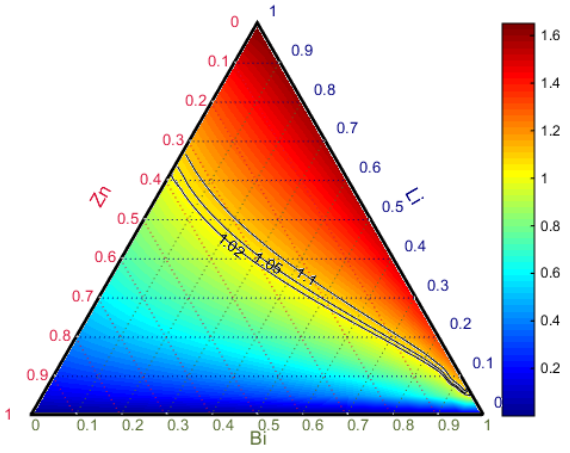
Zn
Li
Bi
1.02
1.05
1.1
1.6
1.4
1.2
1
0.8
0.6
0.4
0.2

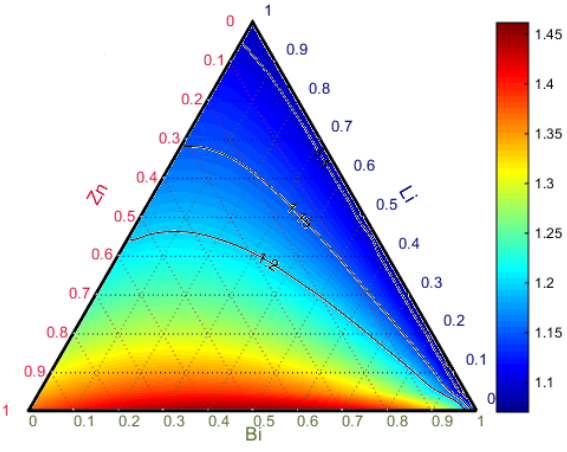
Zn
Li
Bi
1.05
1.2
1.45
1.4
1.35
1.3
1.25
1.2
1.15
1.1

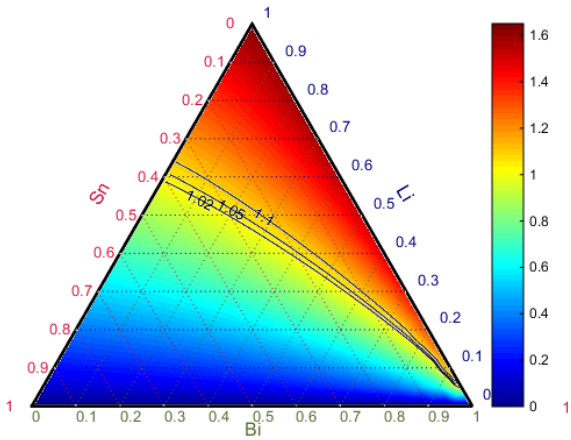
Sn
Li
Bi
1.62
1.05
1
1.6
1.4
1.2
1
0.8
0.6
0.4
0.2
0

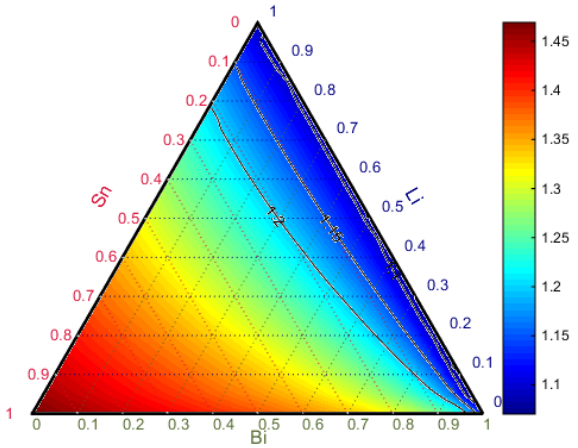
Sn
Li
Bi
1.2
1.45
1.4
1.35
1.3
1.25
1.2
1.15
1.1

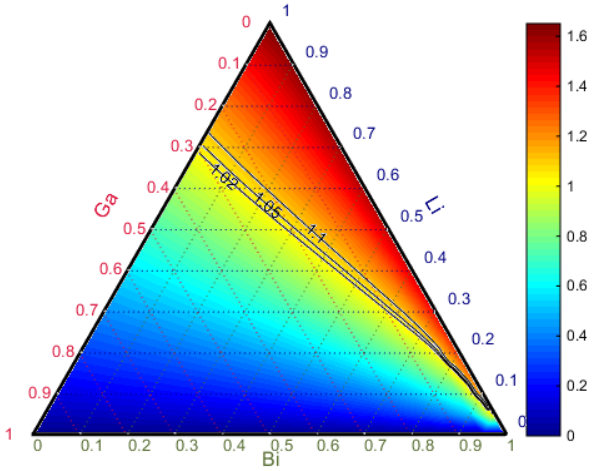
Ga
Li
Bi
1.02
1.05
1
1.6
1.4
1.2
1
0.8
0.6
0.4
0.2
0

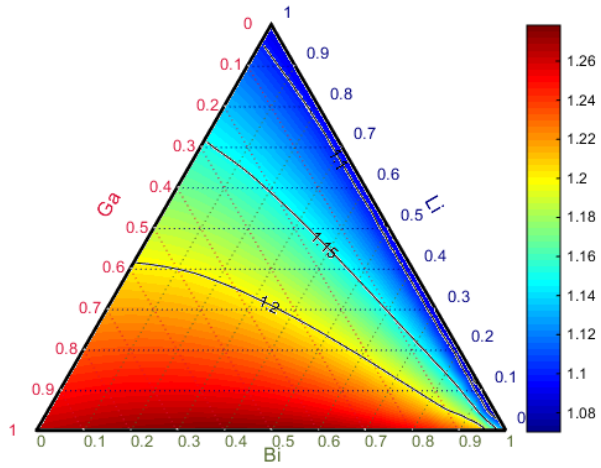
Ga
Li
Bi
1.15
1.2
1.26
1.24
1.22
1.2
1.18
1.16
1.14
1.12
1.1
1.08

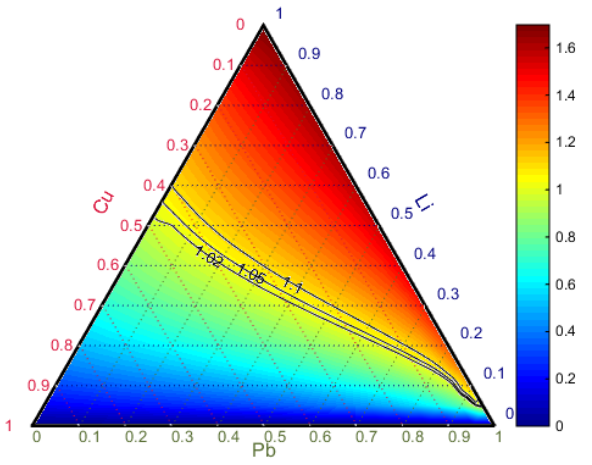
Cu
Li
Pb
1.02
1.05
1
1.6
1.4
1.2
1
0.8
0.6
0.4
0.2
0

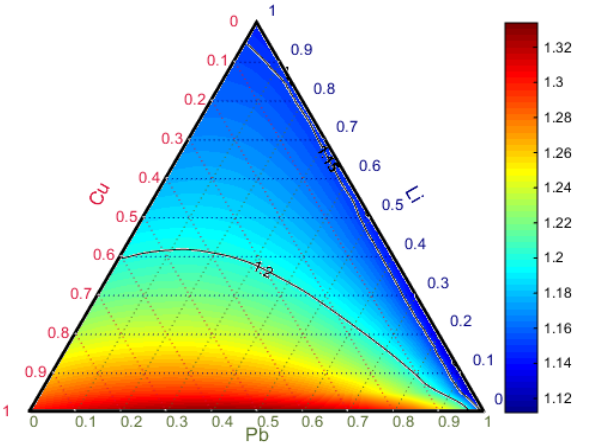
Cu
Li
Pb
1.15
1.2
1.32
1.3
1.28
1.26
1.24
1.22
1.2
1.18
1.16
1.14
1.12

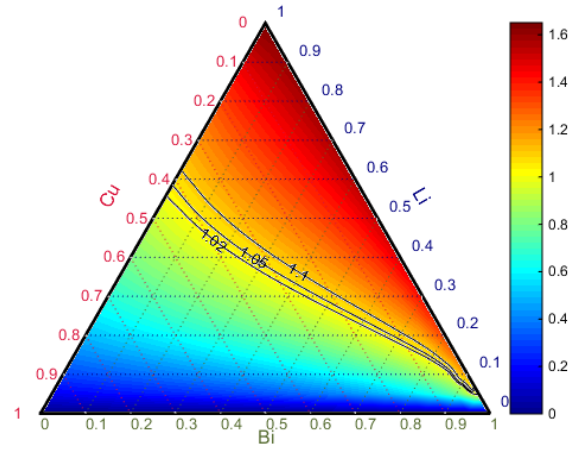
Cu
Li
Bi
1.02
1.05
1.1

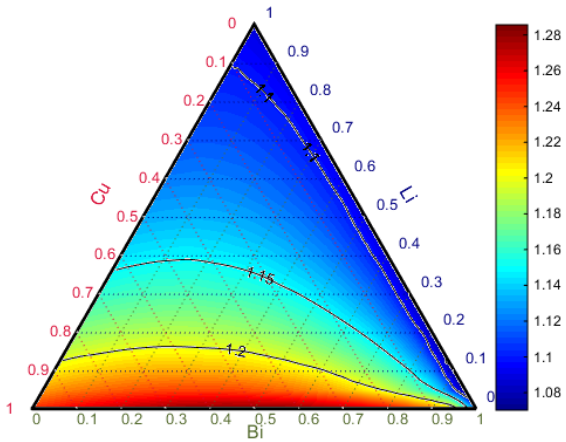
Cu
Li
Bi
1.1
1.15
1.2

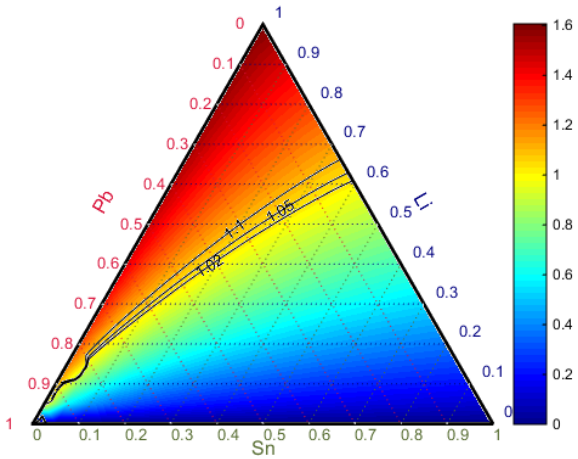
Pb
Li
Sn
1.1
1.05
1.02

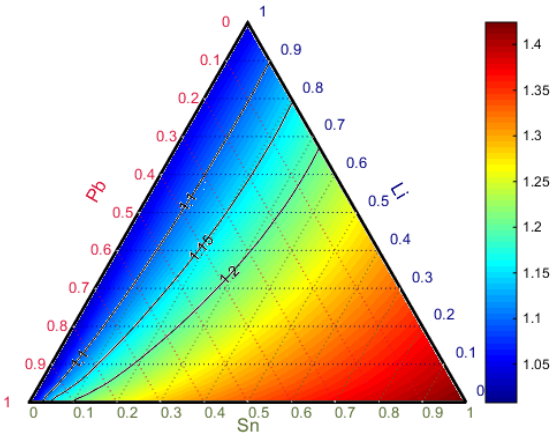
Pb
Li
Sn
1.1
1.15
1.2

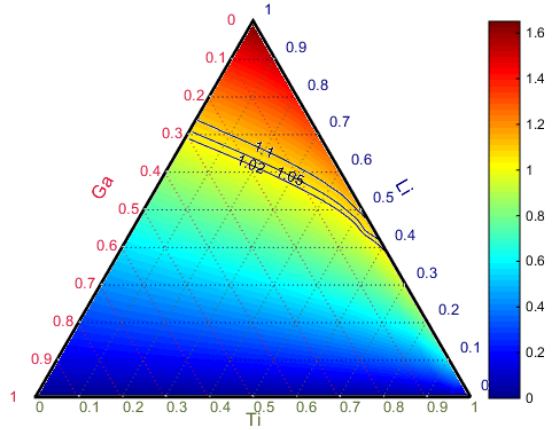
Ga
Li
Ti
1.1
1.02
1.05

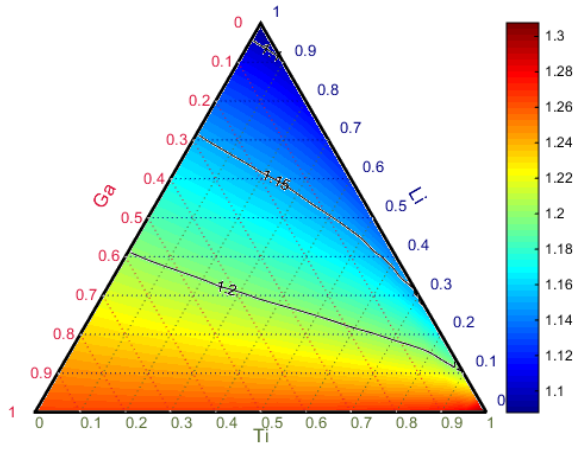
Ga
Li
Ti
1.15
1.2

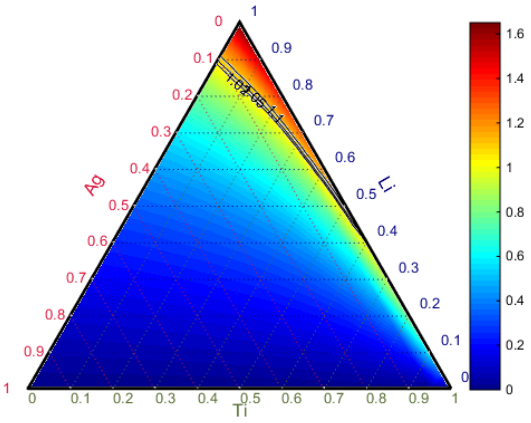
Ag
Cl
Ti
1.03
1.05
1.1

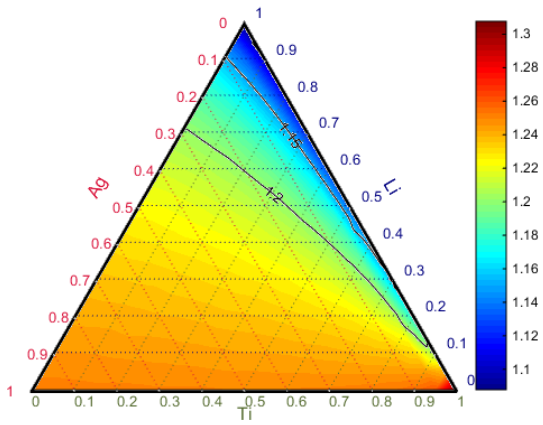
Ag
Cl
Ti
1.15
1.2

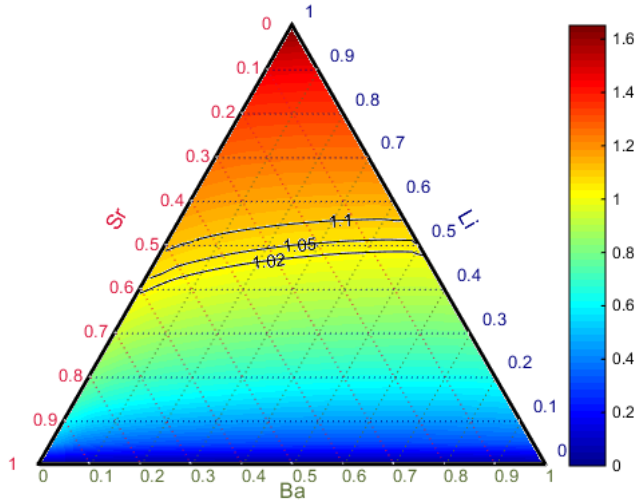
Sr
Cl
Ba
1.02
1.05
1.1

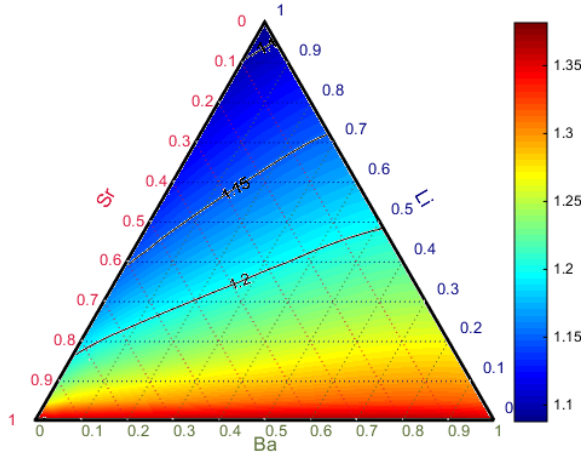
Sr
Cl
Ba
1.15
1.2

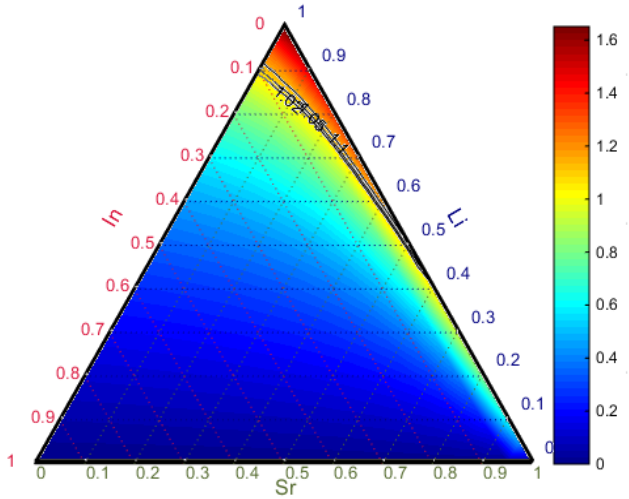
In
Cl
Sr
1.02
1.05
1.1

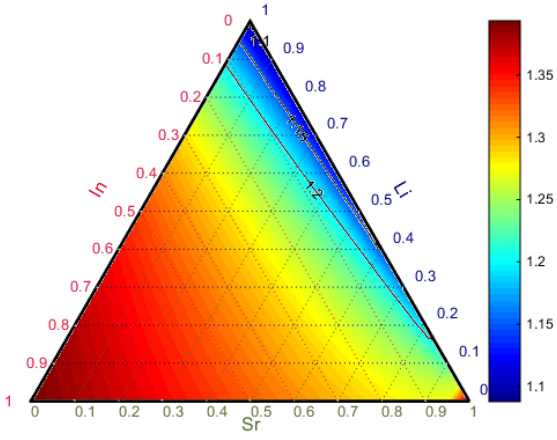
In
Cl
Sr
1.15
1.2

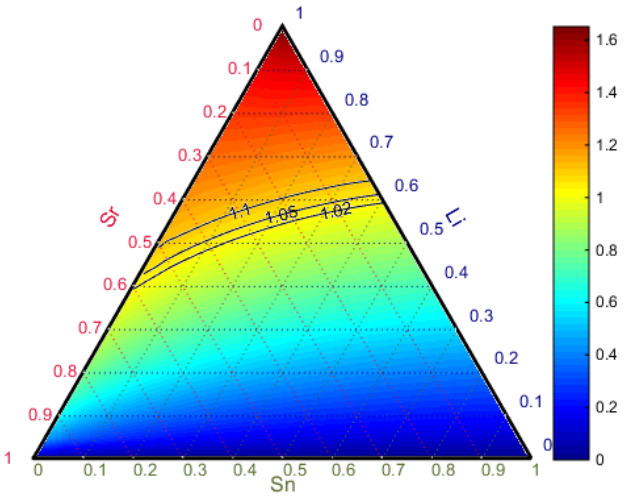
Sr
Sn
Cr
1.1
1.05
1.02

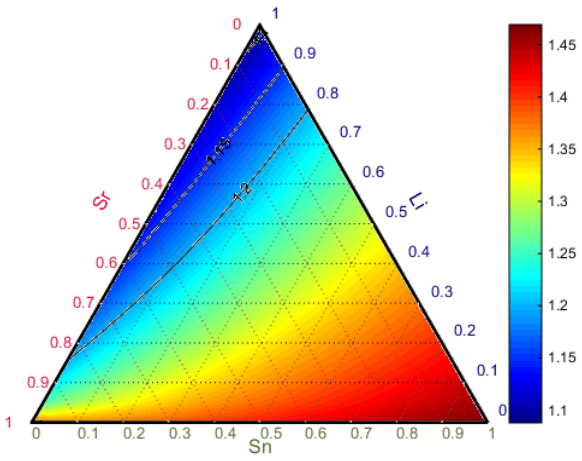
Sr
Sn
Cr
1.15
1.2

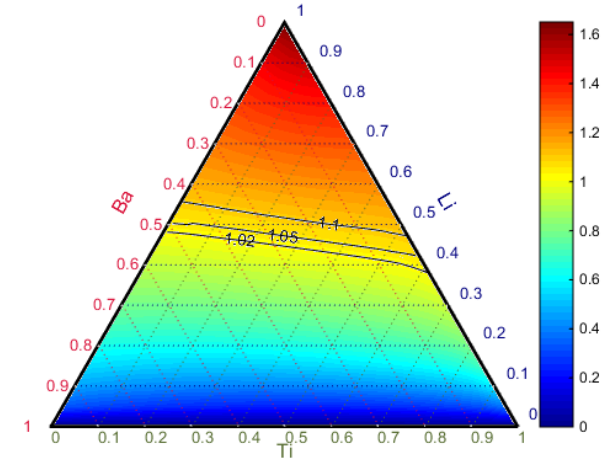
Ba
Ti
Cr
1.1
1.05
1.02

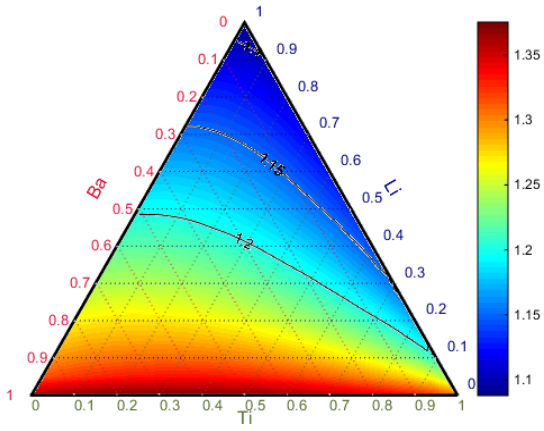
Ba
Ti
Cr
1.15
1.2

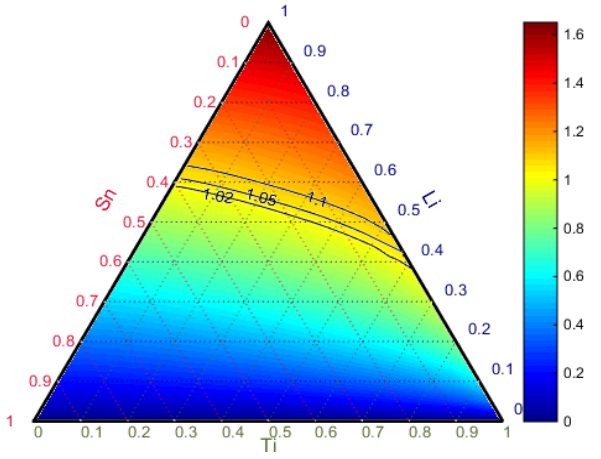
Sn
Ti
Cr
1.02
1.05
1.1

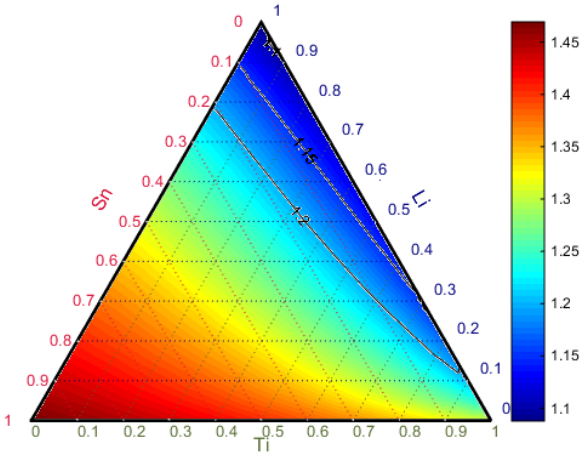
Sn
Ti
Cr
1.15
1.2

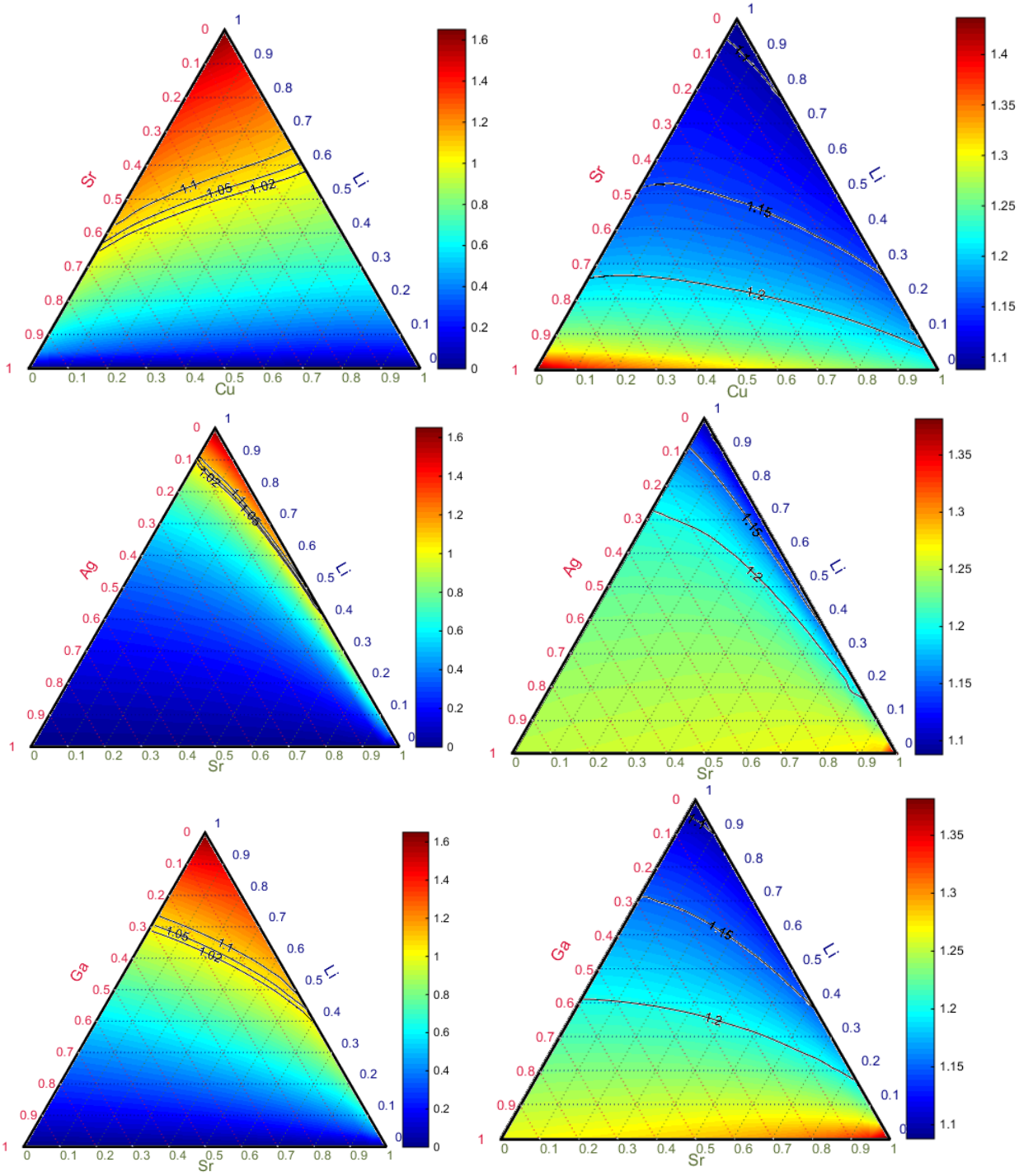
Sr
Cu
1.1
1.05
1.02
Cu
1.15
1.2
Ag
Sr
1.02
1.1
1.05
Sr
1.15
1.2
Ga
Sr
1.05
1.1
1.02
Sr
1.15
1.2

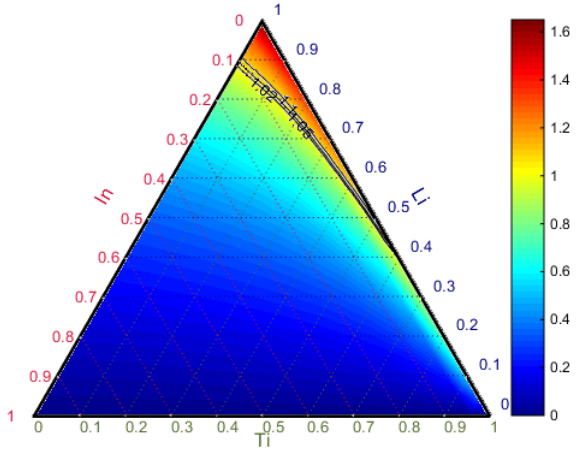
In
Ti
Cl
1.02
1.05
1.1

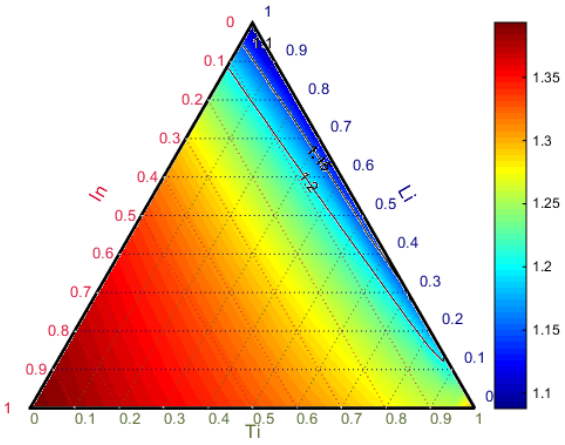
In
Ti
Cl
1.1
1.15
1.2

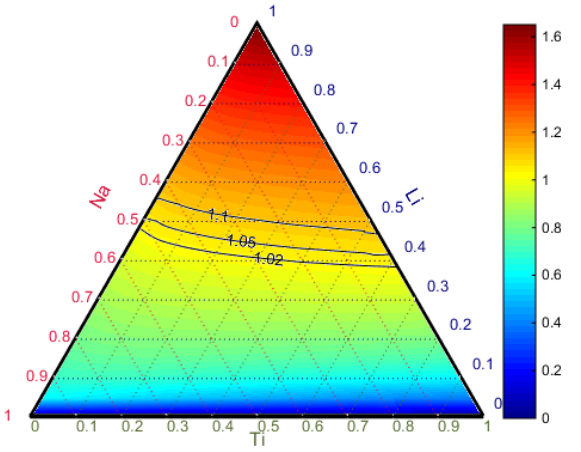
Na
Ti
Cl
1.1
1.05
1.02

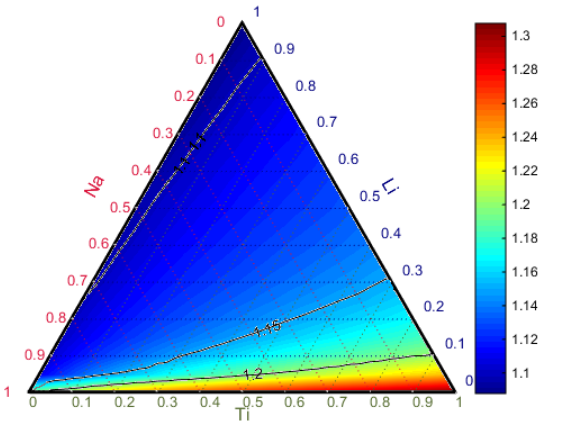
Na
Ti
Cl
1.1
1.15
1.2

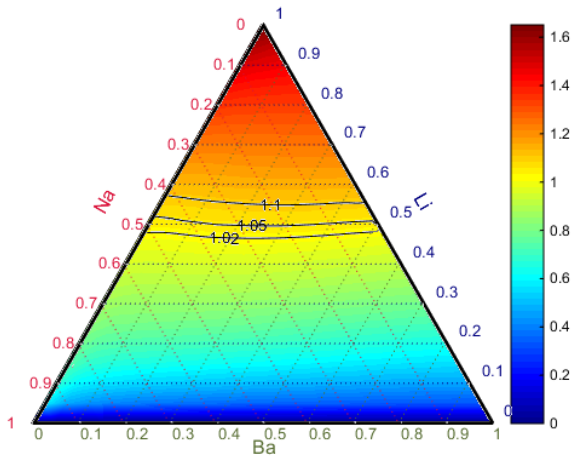
Na
Ba
Cl
1.1
1.05
1.02

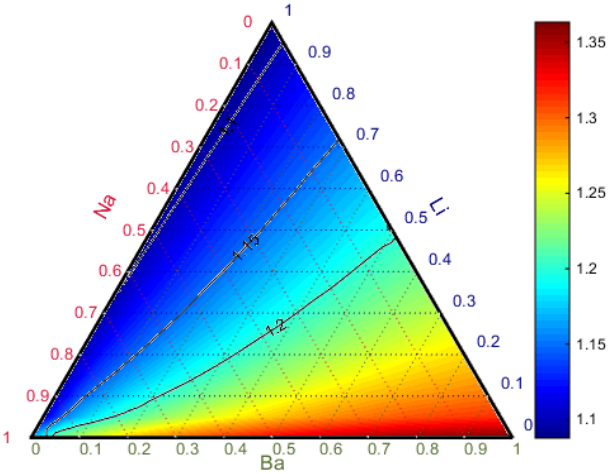
Na
Ba
Cl
1.15
1.2

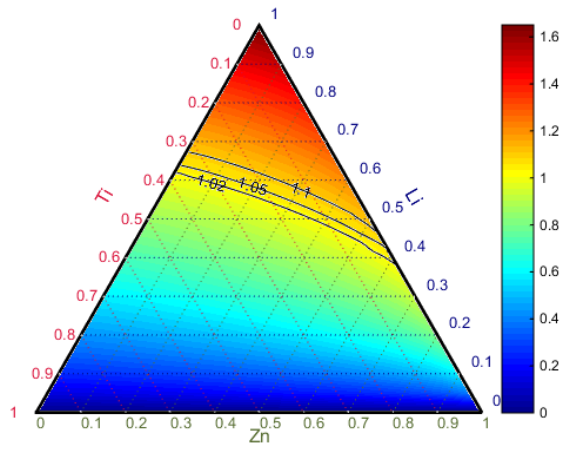
Ti
Zn
Cl
1.02
1.05
1.1

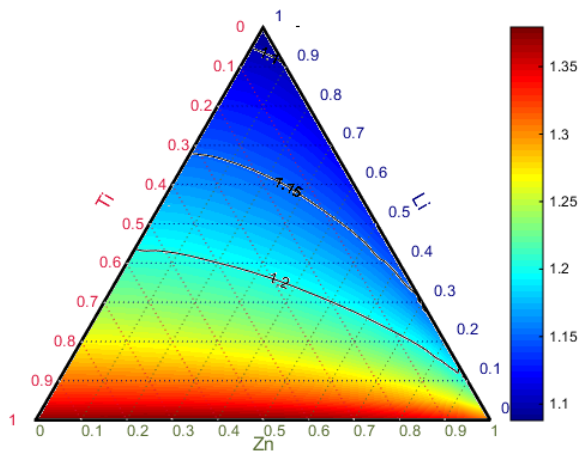
Ti
Zn
Cl
1.15
1.2

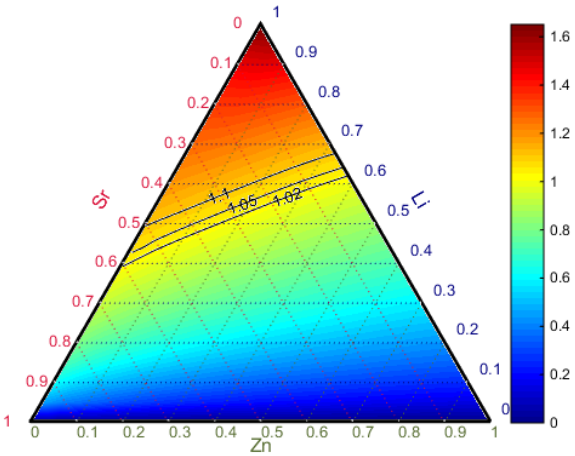
Sr
Zn
Cl
1.1
1.05
1.02

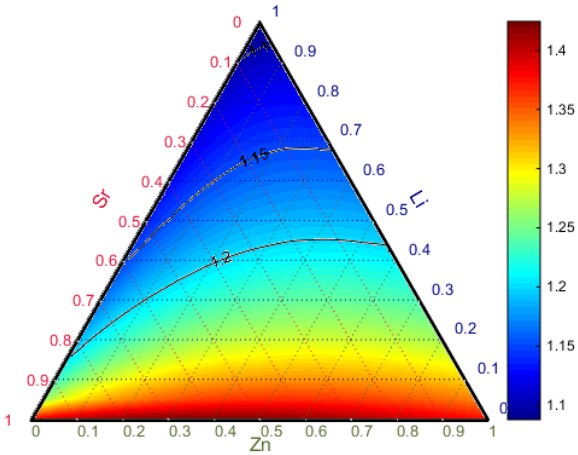
Sr
Zn
Cl
1.15
1.2

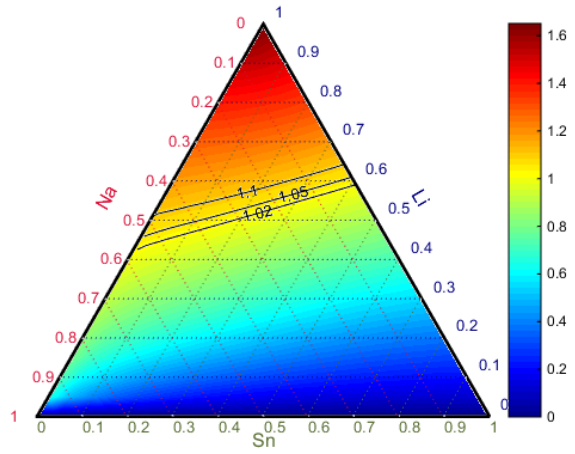
Na
Sn
Cl
1.1
1.05
1.02

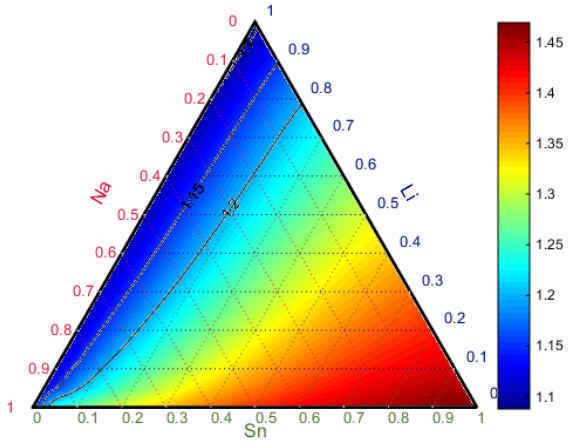
Na
Sn
Cl
1.15
1.2

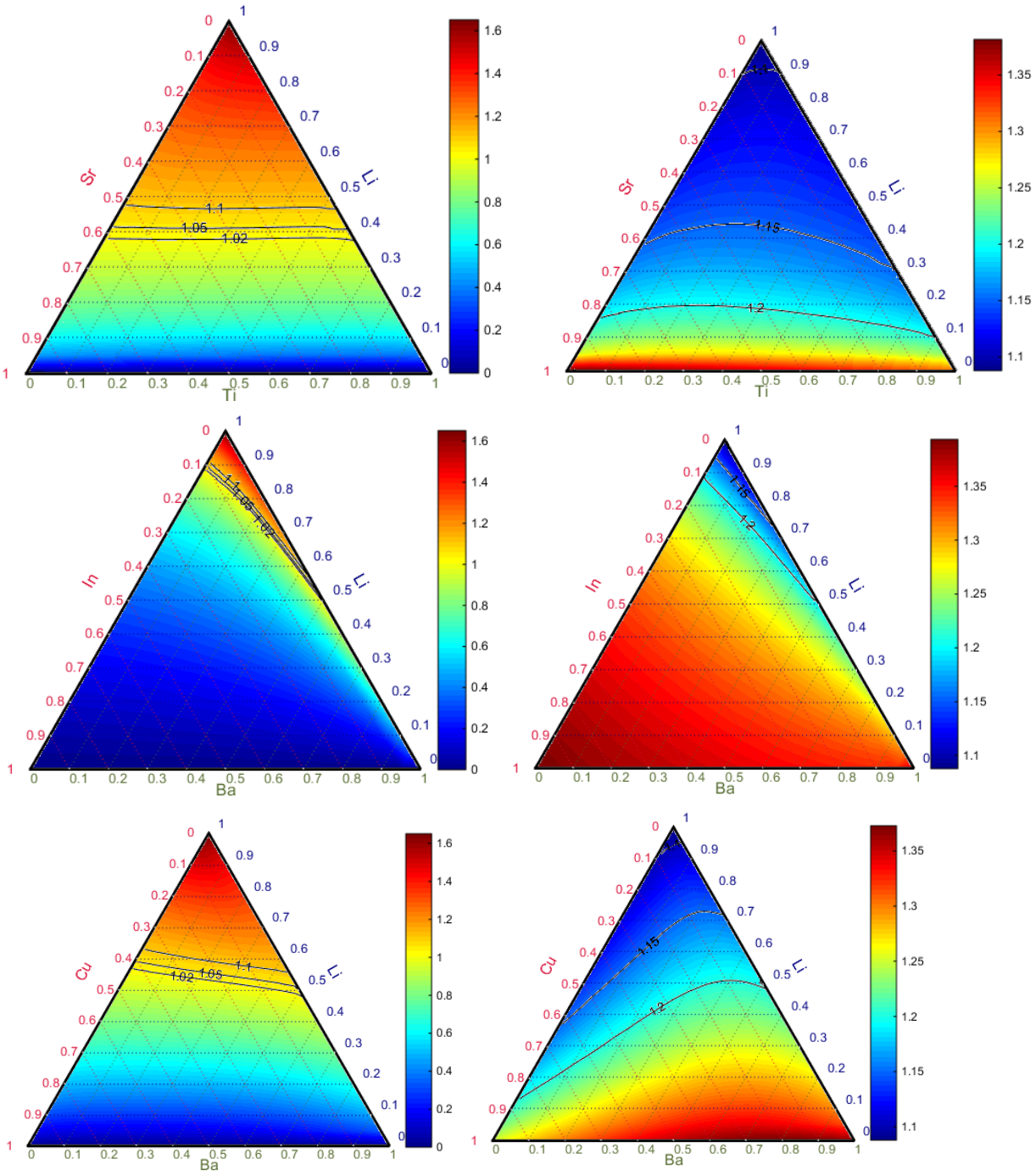
Sr
Ti
Li
1.1
1.05
1.02
1.6
1.4
1.2
1
0.8
0.6
0.4
0.2
0
Sr
Ti
Li
1.15
1.2
1.35
1.3
1.25
1.2
1.15
1.1
In
Ba
Li
1.1
1.05
1.02
1.6
1.4
1.2
1
0.8
0.6
0.4
0.2
0
In
Ba
Li
1.15
1.2
1.35
1.3
1.25
1.2
1.15
1.1
Cu
Ba
Li
1.1
1.05
1.02
1.6
1.4
1.2
1
0.8
0.6
0.4
0.2
0
Cu
Ba
Li
1.15
1.2
1.35
1.3
1.25
1.2
1.15
1.1

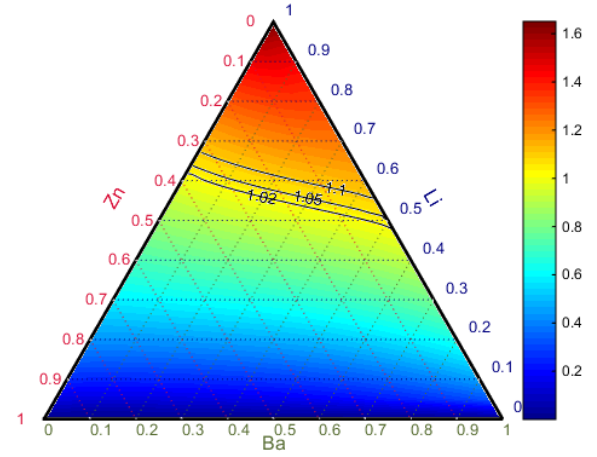
Zn
Li
Ba
1.02
1.05
1.1

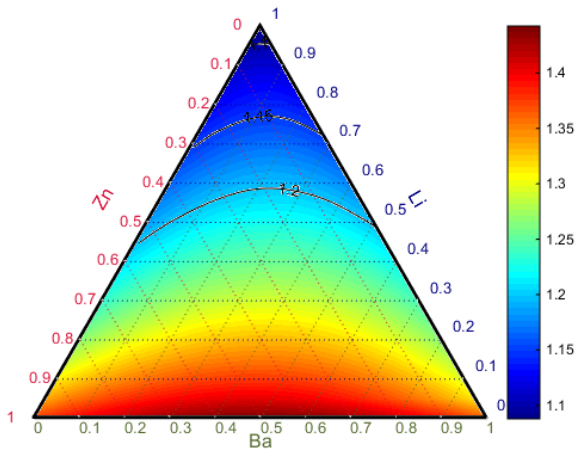
Zn
Li
Ba
1.45
1.2

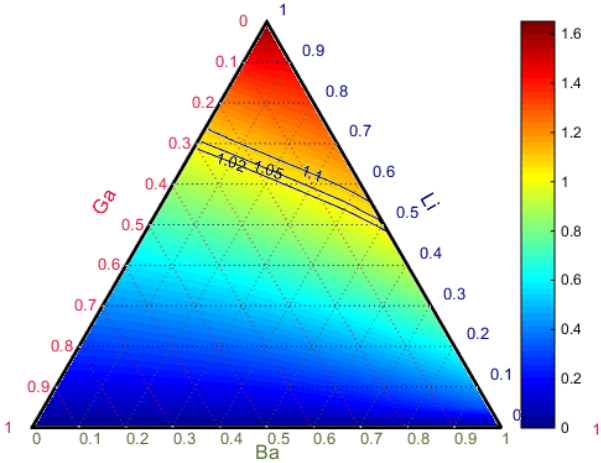
Ga
Li
Ba
1.02
1.05
1.1

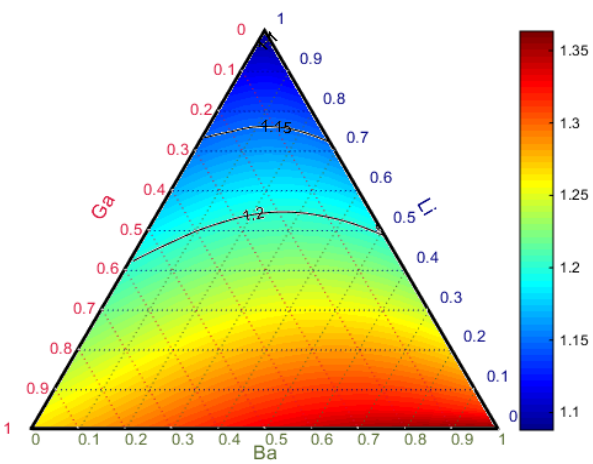
Ga
Li
Ba
1.15
1.2

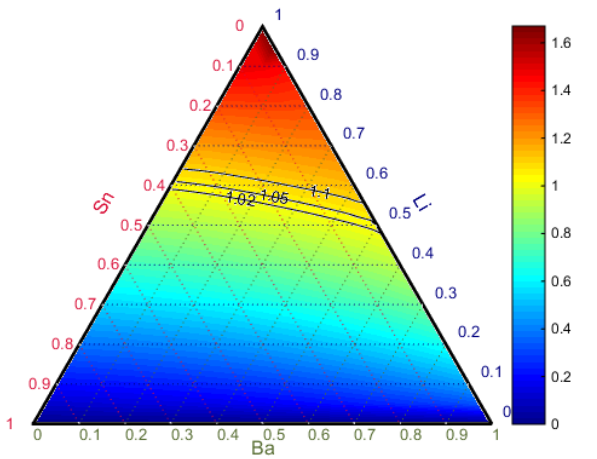
Sn
Li
Ba
1.02
1.05
1.1

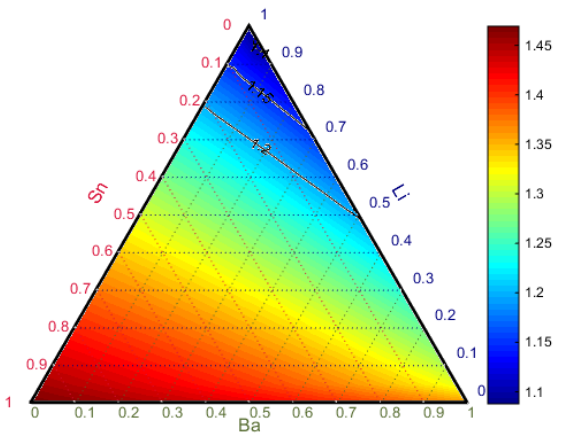
Sn
Li
Ba
1.15
1.2

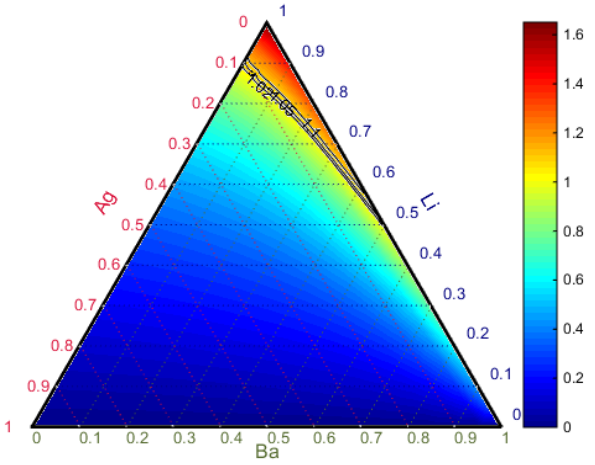
Ag
Ba
Cl
1.02
1.05
1.1

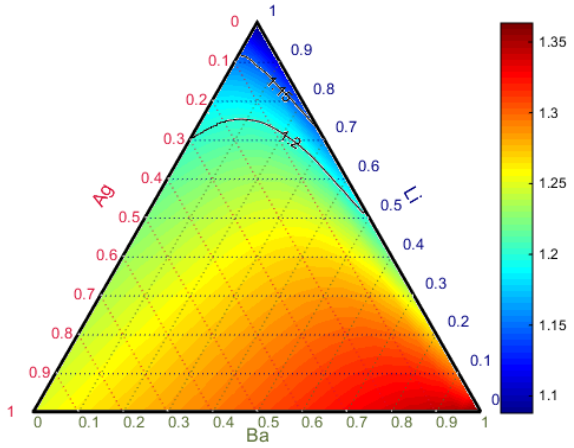
Ag
Ba
Cl
1.15
1.2

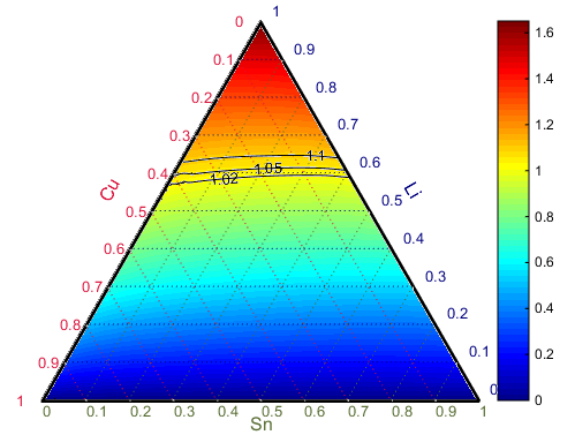
Cu
Sn
Cl
1.02
1.05
1.1

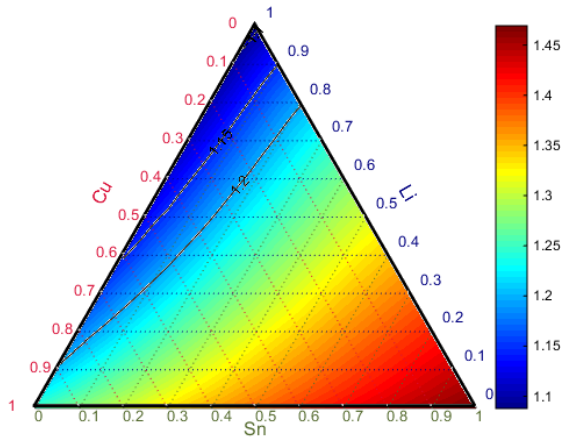
Cu
Sn
Cl
1.15
1.2

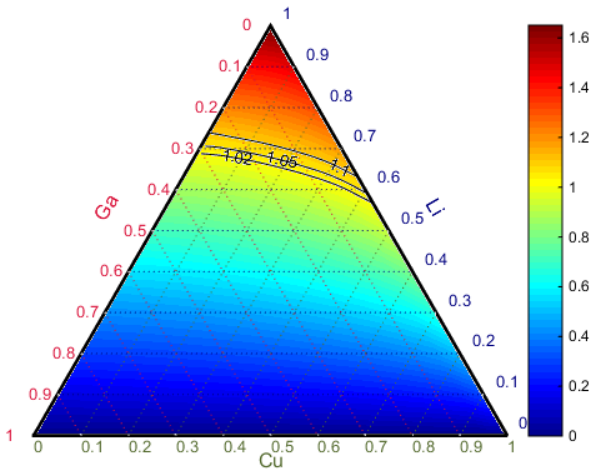
Ga
Cu
Cl
1.02
1.05
1.1

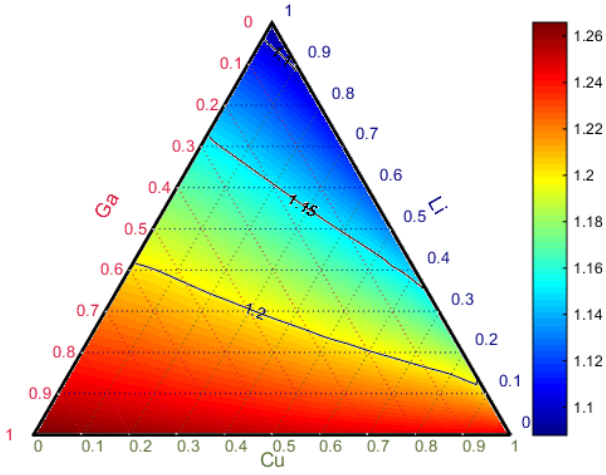
Ga
Cu
Cl
1.15
1.2

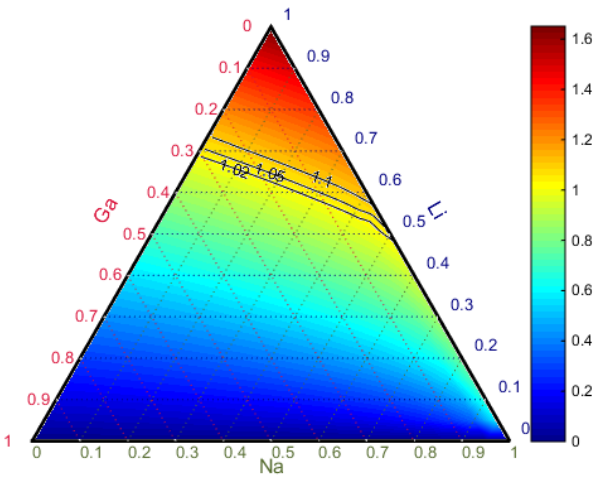
Ga
Li
Na
1.02
1.05
1.1

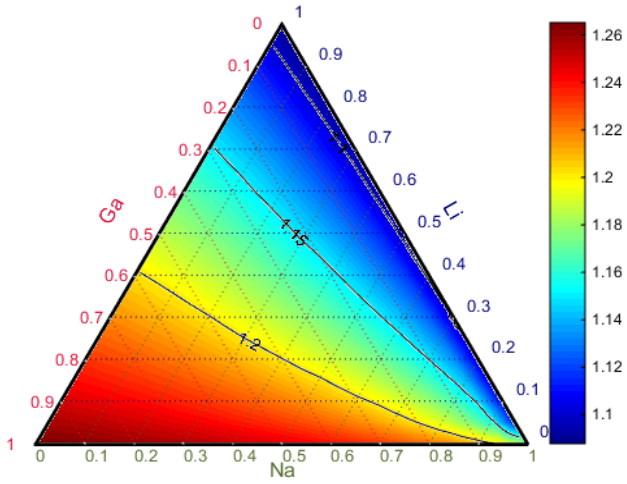
Ga
Li
Na
1.15
1.2

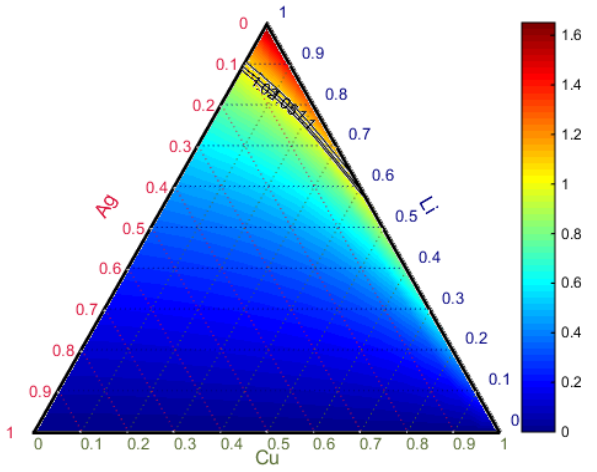
Ag
Li
Cu
1.02
1.05
1.1

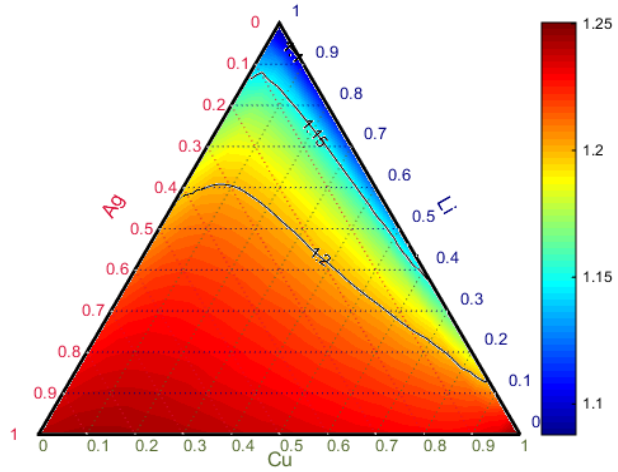
Ag
Li
Cu
1.15
1.2

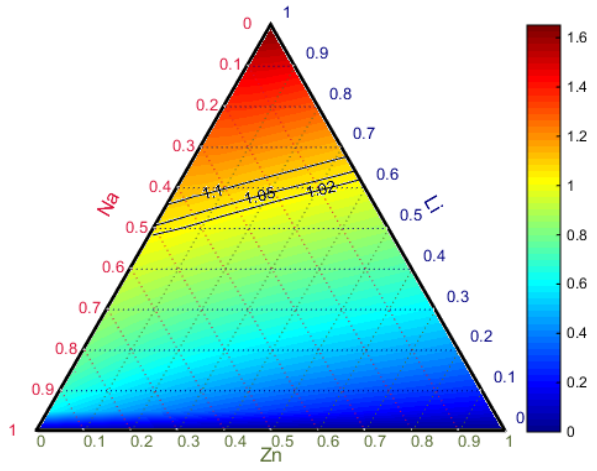
Na
Li
Zn
1.1
1.05
1.02

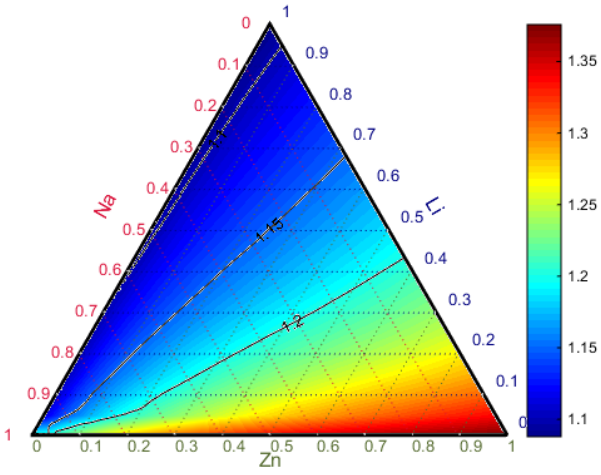
Na
Li
Zn
1.15
1.2

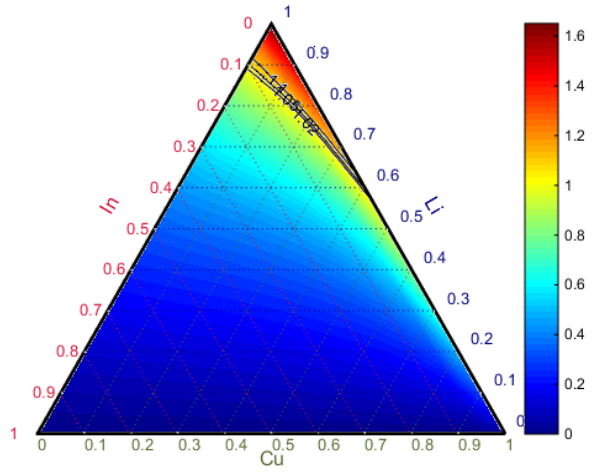
In
Li
Cu
1.02
1.05
1.1

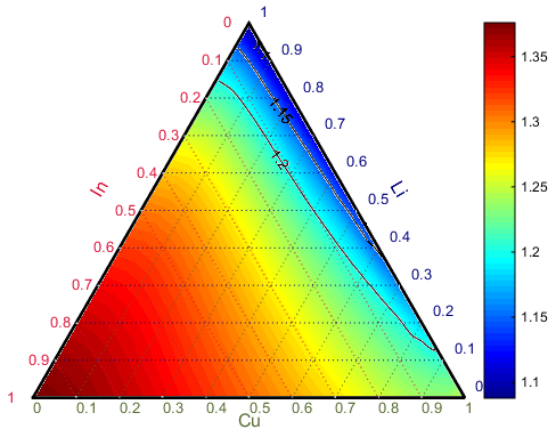
In
Li
Cu
1.15
1.2

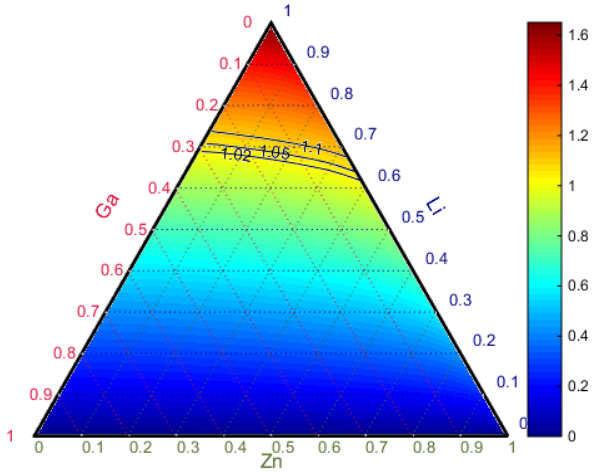
Ga
Li
Zn
1.02
1.05
1.1

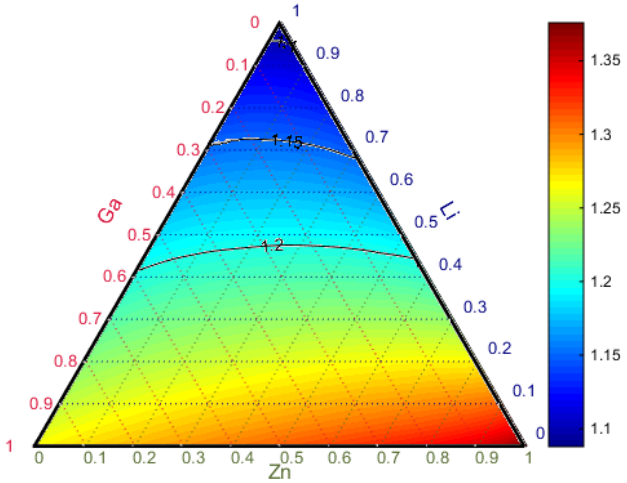
Ga
Li
Zn
1.15
1.2

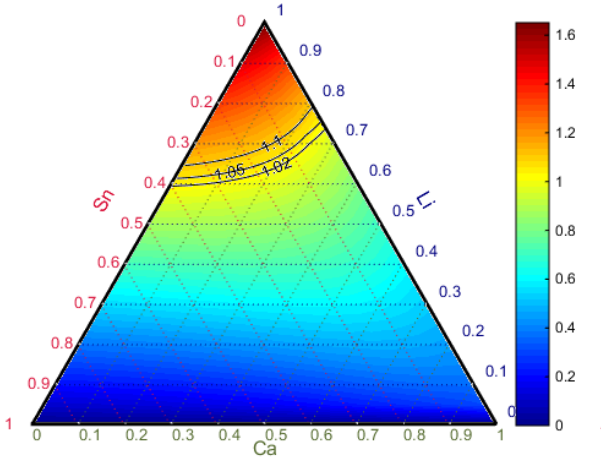
Sn
Li
Ca
1.02
1.05
1.1

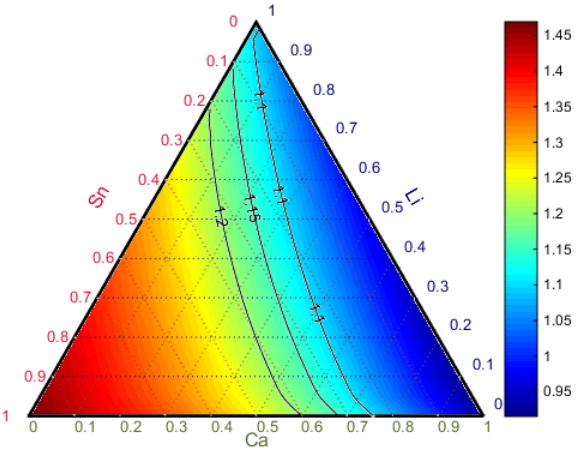
Sn
Li
Ca
1.1
1.15
1.2

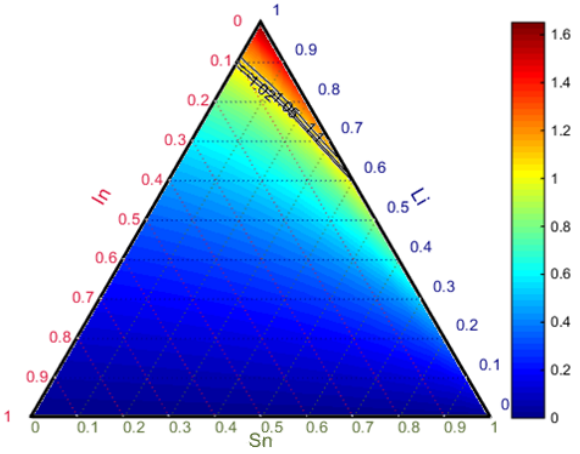
In
Sn
Cl
1.02
1.05
1.1

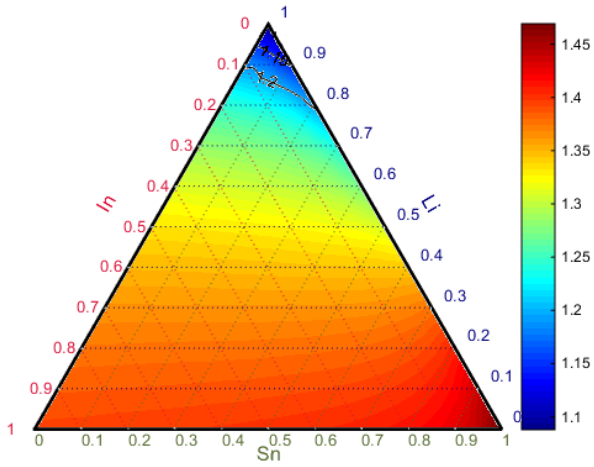
In
Sn
Cl
1.15
1.2

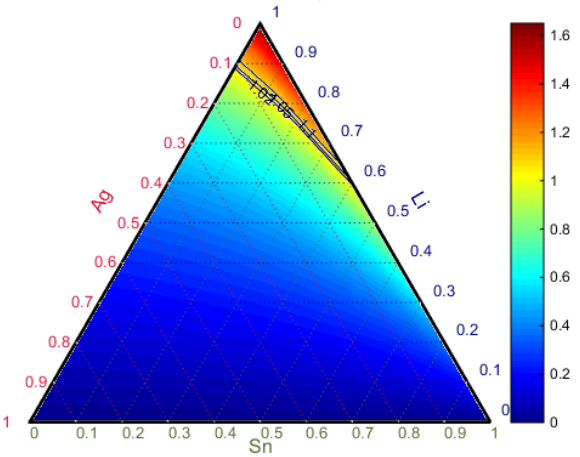
Ag
Sn
Cl
1.02
1.05
1.1

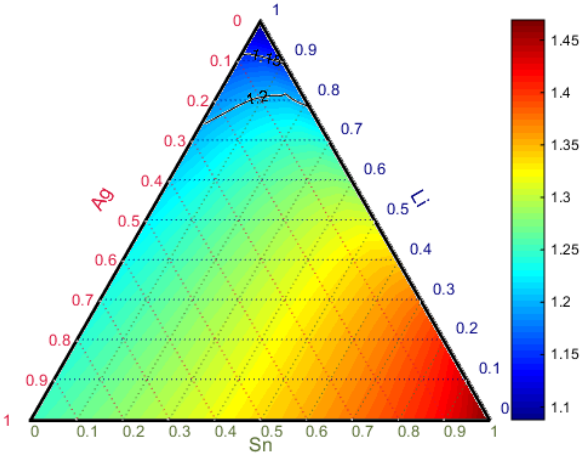
Ag
Sn
Cl
1.15
1.2

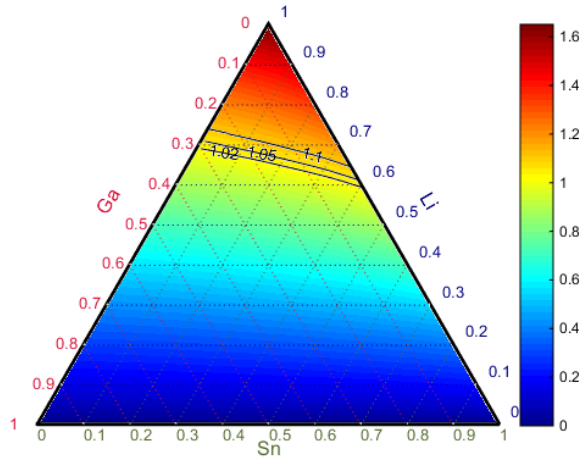
Ga
Sn
Cl
1.02
1.05
1.1

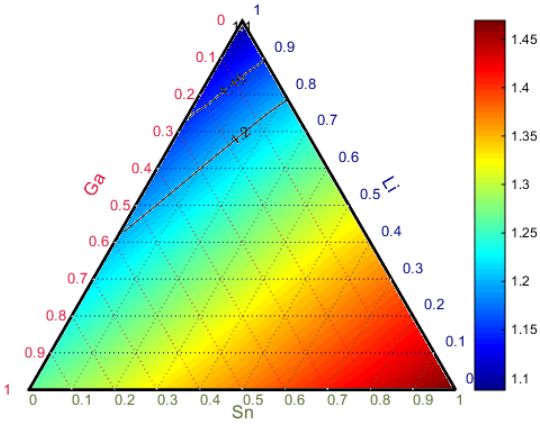
Ga
Sn
Cl
1.15
1.2

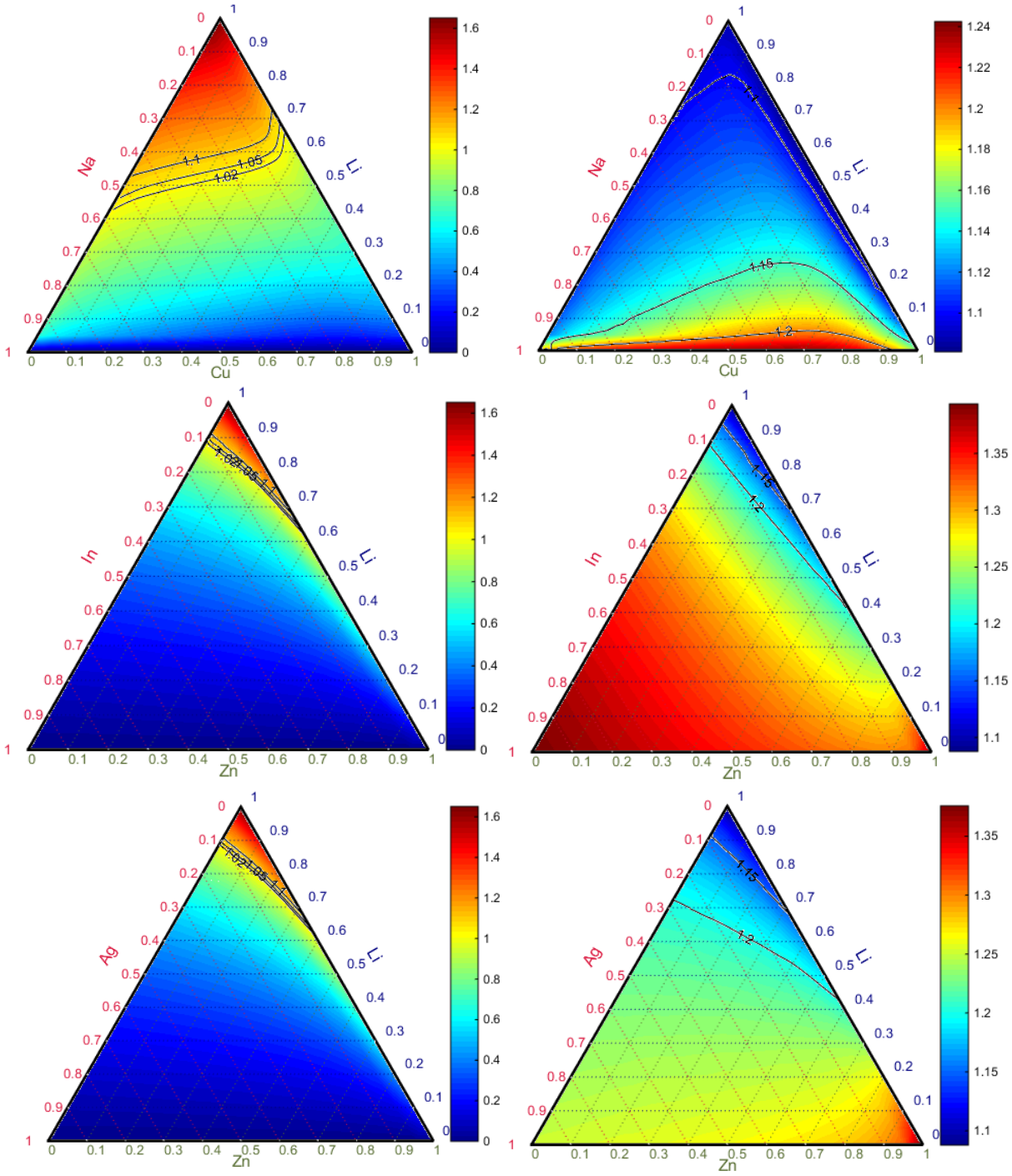
Na
Li
Cu
1.4
1.05
1.02
In
Zn
1.02
1.05
1.1
1.15
1.2
Ag
Zn
1.02
1.05
1.1
1.15
1.2

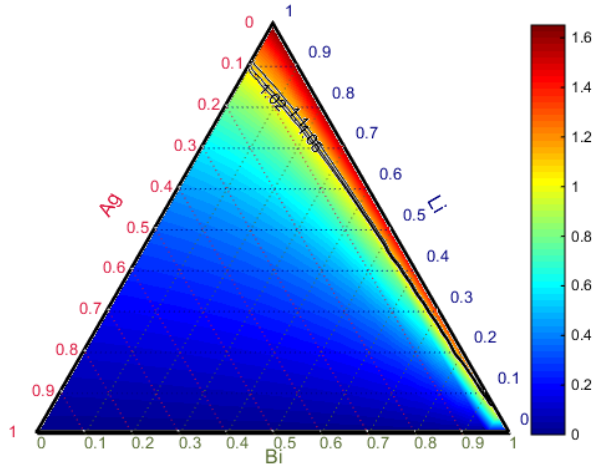
Ag
Bi
Li
1.02
1.05
1.1

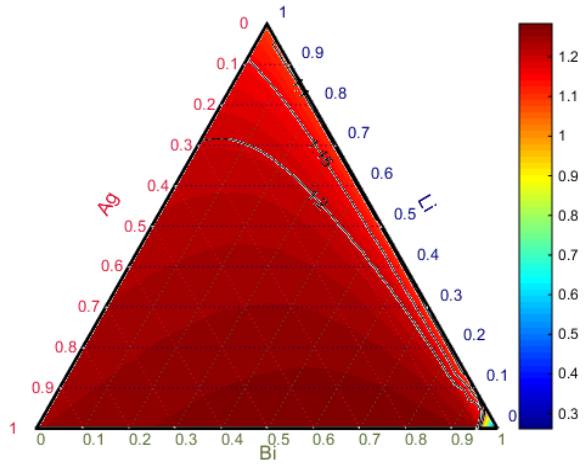
Ag
Bi
Li
1.15
1.2

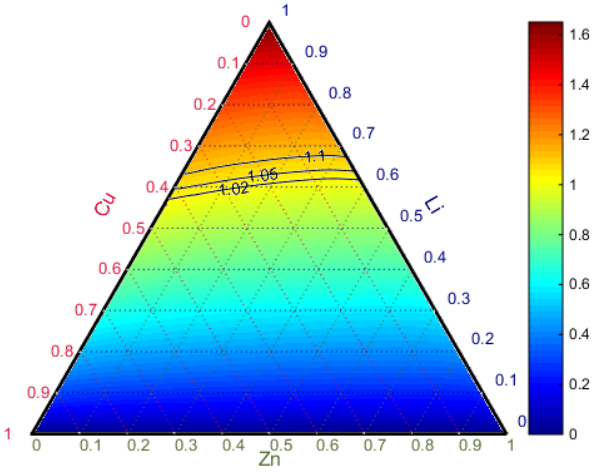
Cu
Zn
Li
1.02
1.05
1.1

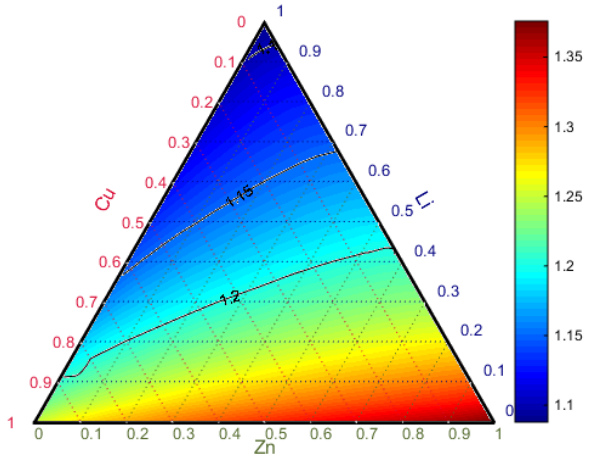
Cu
Zn
Li
1.15
1.2